1521-009X/41/6/1195–1210$25.00
Drug Metabolism and Disposition
http://dx.doi.org/10.1124/dmd.112.050310
Drug Metab Dispos 41:1195–1210, June 2013

Metabolism and Pharmacokinetics of Novel Selective Vascular Endothelial Growth Factor Receptor-2 Inhibitor Apatinib in Humans[S]

Juefang Ding, Xiaoyan Chen, Zhiwei Gao, Xiaojian Dai, Liang Li, Cen Xie, Haoyuan Jiang, Lijia Zhang, and Dafang Zhong

Shanghai Institute of Materia Medica, Chinese Academy of Sciences, Shanghai, China (J.D., X.C., Z.G., X.D., L.L., C.X., D.Z.); and Jiangsu Hengrui Medicine Co. Ltd., Lianyungang, China (H.J., L.Z.)

Received November 26, 2012; accepted March 18, 2013

ABSTRACT

Apatinib is a new oral antiangiogenic molecule that inhibits vascular endothelial growth factor receptor-2. The present study aimed to determine the metabolism, pharmacokinetics, and excretion of apatinib in humans and to identify the enzymes responsible for its metabolism. The primary routes of apatinib biotransformation included *E*- and *Z*-cyclopentyl-3-hydroxylation, *N*-dealkylation, pyridyl-25-*N*-oxidation, 16-hydroxylation, dioxygenation, and *O*-glucuronidation after 3-hydroxylation. Nine major metabolites were confirmed by comparison with reference standards. The total recovery of the administered dose was 76.8% within 96 hours postdose, with 69.8 and 7.02% of the administered dose excreted in feces and urine, respectively. About 59.0% of the administered dose was excreted unchanged via feces. Unchanged apatinib was detected in negligible quantities in urine, indicating that systemically available apatinib was extensively metabolized. The major circulating metabolite was the pharmacologically inactive *E*-3-hydroxy-apatinib-*O*-glucuronide (M9-2), the steady-state exposure of which was 125% that of the apatinib. The steady-state exposures of *E*-3-hydroxy-apatinib (M1-1), *Z*-3-hydroxy-apatinib (M1-2), and apatinib-25-*N*-oxide (M1-6) were 56, 22, and 32% of parent drug exposure, respectively. Calculated as pharmacological activity index values, the contribution of M1-1 to the pharmacology of the drug was 5.42 to 19.3% that of the parent drug. The contribution of M1-2 and M1-6 to the pharmacology of the drug was less than 1%. Therefore, apatinib was a major contributor to the overall pharmacological activity in humans. Apatinib was metabolized primarily by CYP3A4/5 and, to a lesser extent, by CYP2D6, CYP2C9, and CYP2E1. UGT2B7 was the main enzyme responsible for M9-2 formation. Both UGT1A4 and UGT2B7 were responsible for *Z*-3-hydroxy-apatinib-*O*-glucuronide (M9-1) formation.

Introduction

New blood vessel formation (angiogenesis) is a critical step for tumor cell survival, proliferation, local invasion, and metastasis (Carmeliet and Jain, 2000). Vascular endothelial growth factor receptors (VEGFRs) are receptor tyrosine kinases (RTKs) that function as key regulators of this process. The VEGFR-family proteins consist of three members: VEGFR-1 (Flt-1), VEGFR-2 (KDR/Flk-1), and VEGFR-3 (Flt-4), among which VEGFR-2 is thought to be principally responsible for angiogenesis in malignancies (Glade-Bender et al., 2003). Small-molecule VEGFR inhibitors are widely used for the treatment of metastatic renal cell carcinoma, gastrointestinal stromal tumors, hepatocellular carcinoma (Ivy et al., 2009), soft tissue sarcoma (Gennigens and Jerusalem, 2012), and medullary thyroid cancer (Degrauwe et al., 2012) and in the development of a number of other oncology indications, including colorectal cancer, non-small-cell lung cancer, pancreatic cancer, ovarian cancer, and breast cancer (Ivy et al., 2009).

Apatinib (*N*-[4-(1-cyano-cyclopentyl)phenyl]-2-(4-pyridylmethyl)amino-3-pyridine carboxamide, formerly known as YN968D1) is an orally administered small-molecule RTK inhibitor that selectively targets VEGFR-2 with an IC_{50} of approximately 1 nM. Apatinib also less effectively inhibits the activities of platelet-derived growth factor-β (PDGFR-β), c-kit, and c-src, all of which have been implicated in the pathogenesis of human tumors (Irby and Yeatman, 2000; Heinrich et al., 2002; Song et al., 2005). Apatinib shows antitumor efficacy, with good tolerance, in mice when administered alone or in combination with chemotherapeutic drugs against a broad range of human tumor xenografts (Tian et al., 2011).

Apatinib reverses P-glycoprotein (ABCB1)- and ABCG2-mediated multidrug resistance in drug-resistant solid tumor cells by inhibiting their transport function (Mi et al., 2010). It also targets to side population cells and ABCB1-overexpressing leukemia cells to enhance

dx.doi.org/10.1124/dmd.112.050310.
[S] This article has supplemental material available at dmd.aspetjournals.org.

ABBREVIATIONS: ABT, 1-aminobenzotriazole; AUC, area under the concentration-time curve; AZD0328, (29R)-spiro[1-azabicyclo[2.2.2]octane-3,29(39H)-furo[2,3-b]pyridine]; CE, collision energy; CL_{int}, intrinsic clearance; C_{max}, peak plasma concentration; FMO, flavin-containing mono-oxygenase; HIM, human intestinal microsome; HLM, human liver microsome; HPLC, high performace liquid chromatography; HPM, human pulmonary microsome; HRM, human renal microsome; LC-MS/MS, liquid chromatography-tandem mass spectrometry; *m/z*, mass-to-charge ratio; P450, cytochrome P450; PAI, pharmacological activity index; PDGFR-β, platelet-derived growth factor receptor-β; Q-TOF MS, quadrupole time-of-flight mass spectrometer; RTK, receptor tyrosine kinase; T_{max}, time to reach peak plasma concentration; UDPGA, uridine 5′-diphosphoglucuronic acid; $TiCl_3$, titanium trichloride; UGT, UDP-glucuronosyltransferase; UPLC, ultra performance liquid chromatography; VEGFR-2, vascular endothelial growth factor receptor-2; XIC, extracted ion chromatogram.

the efficacy of chemotherapeutic drugs (Tong et al., 2012). These results suggest that apatinib may be used in combination with conventional ABCB1 and ABCG2 substrate chemotherapeutic drugs to overcome multidrug resistance in clinical cancer chemotherapy.

The results from a phase 1 clinical study conducted in patients with advanced solid tumors have shown that apatinib can be well tolerated and exhibits substantial antitumor activity across a broad range of malignancies at the recommended dose of 750 mg once daily (Li et al., 2010). The pharmacokinetic parameters of apatinib in plasma were also calculated using noncompartmental analysis. Apatinib is currently being evaluated in phase 2/3 clinical trials for the treatment of many advanced cancer types, including gastric carcinoma, hepatocellular carcinoma, breast cancer, and colorectal cancer.

Absorption, distribution, metabolism, and excretion studies have become an integral and critical part of drug development. The present study was undertaken to assess the metabolic profile, routes of excretion, and pharmacokinetics of apatinib in humans after single- or multiple-dose administration of 750 mg of apatinib mesylate tablets (corresponding to 604 mg of apatinib free base). Cytochrome P450 (P450) isozymes responsible for the oxidative metabolism of apatinib, as well as UDP-glucuronosyltransferase (UGT) isozymes involved in the *O*-glucuronidation of hydroxylated metabolites of apatinib, were also examined to help predict potential drug-drug interaction and variability in pharmacokinetics.

Materials and Methods

Chemicals

Apatinib mesylate tablets were manufactured by Jiangsu Hengrui Medicine Co., Ltd. (Lianyungang, China) and used for clinical trials. Reference standards of apatinib mesylate, *E*-3-hydroxy-apatinib (M1-1), *Z*-3-hydroxy-apatinib (M1-2), and vatalanib (internal standard for pharmacokinetic study) were also provided by Hengrui Medicine. The reference standard of apatinib-25-*N*-oxide (M1-6) was synthesized and purified in our laboratory. Reference standards of *Z*-3-hydroxy-16-hydroxy-*N*-dealkylated metabolite (M4-7), *E*-3-hydroxy-16-hydroxy-*N*-dealkylated metabolite (M4-8), *Z*-3-hydroxy-25-*N*-oxide metabolite (M6-9), *E*-3-hydroxy-25-*N*-oxide metabolite (M6-10), *E*-3-hydroxy-*O*-glucuronide-*N*-dealkylated metabolite (M8-2), and *E*-3-hydroxy-apatinib-*O*-glucuronide (M9-2) were isolated and purified from human urine in our laboratory. The following chemicals were purchased from Sigma-Aldrich (St. Louis, MO): NADPH, alamethicin, uridine 5′-diphosphoglucuronic acid (UDPGA), β-glucuronidase from *Helix pomatia* (type H-3), 1-aminobenzotriazole (ABT), sulfaphenazole, ticlopidine, quinidine, ketoconazole, chlormethiazole, racemic flurbiprofen, mefenamic acid, hecogenin, and all high-performance liquid chromatography (HPLC)-grade solvents used for ultra performance liquid chromatography-UV/quadrupole time-of-flight mass spectrometry (UPLC-UV/Q-TOF MS) and liquid chromatography-tandem mass spectrometry (LC-MS/MS) analysis. Other reagents used were of analytical grade (Sinopharm Chemical Reagent Co. Ltd, Shanghai, China). Deionized water was purified by a Millipore Milli-Q Gradient Water Purification System (Molsheim, France). YMC*GEL ODS-A-HG (12 nm S-50 μM; YMC Co. Ltd., Kyoto, Japan) was used to fractionate the urine samples before further purification.

Enzyme Sources

Pooled human liver microsomes (HLMs), recombinant human P450 isozymes (CYP1A2, CYP1B1, CYP2A6, CYP2B6, CYP2C8, CYP2C9, CYP2C19, CYP2D6, CYP2E1, CYP3A4, CYP3A5, and CYP4A11), recombinant human flavin-containing mono-oxygenases (FMO1, FMO3, and FMO5), and recombinant human UGTs (UGT1A1, UGT1A3, UGT1A4, UGT1A6, UGT1A7, UGT1A8, UGT1A9, UGT1A10, UGT2B4, UGT2B7, UGT2B15, and UGT2B17) were purchased from BD Gentest (Woburn, MA). Pooled human intestinal microsomes (HIMs), human pulmonary microsomes (HPMs), and human renal microsomes (HRMs) were purchased from Xenotech LLC (Lenexa, KS).

Study Design, Dosing, and Sample Collection

Human studies were conducted in accordance with the principles of the Declaration of Helsinki and Good Clinical Practice. Written informed consent was obtained from all subjects before enrollment.

Healthy Subject Study. This was a single-center, nonrandomized, open-label study. The study protocol and informed consent document were approved by the Ethics Committee of Teda International Cardiovascular Hospital (Tianjin, China). Twelve (six men, six women) healthy Chinese subjects with a mean age of 25.6 years (range, 21–29 years) and a mean body mass index of 22.3 kg/m^2 (range, 19.8–24.0 kg/m^2) participated in the study. The subjects were in good health as assessed by physical examination, without histories of drug or alcohol abuse; they were nonsmokers and on no other medication at the time of the study. After at least a 10-hour overnight fast, each subject received a single dose of 750 mg of apatinib mesylate tablets (corresponding to 604 mg of apatinib free base). Urine samples were collected at predose and between 0–4, 4–8, 8–12, 12–24, 24–36, 36–48, 48–72, and 72–96 hours after dosing and stored at −70°C until analysis. Fecal samples were collected at predose and after each bowel movement for up to 96 hours postdose and homogenized with 5 volumes of methanol. The fecal homogenates were stored at −70°C until analysis.

Patient Study. This was a single-center, nonrandomized, open-label study. The study protocol was approved by the Ethics Committee of Fudan University Shanghai Cancer Center (Shanghai, China). Patients with histologically confirmed advanced colorectal cancer for which no standard curative therapy was available were eligible for this study. Patient entry criteria included age 18 years or older; an Eastern Cooperative Oncology Group performance status between 0 and 1; an estimated life expectancy of 3 months or longer; and adequate hematologic, renal, and liver functions. Patients were excluded if they were pregnant or breastfeeding; had a history of brain metastasis, uncontrolled hypertension, coronary disease or other significant cardiovascular disease, gastrointestinal disorder, or other factors that could interfere with drug absorption; were on anticoagulation therapy; had prior therapy with anti-VEGFR-targeting agents; had a history of any other malignancy; or had recent prior chemotherapy, radiotherapy, or surgery.

Twenty (10 men, 10 women) patients with a mean age of 55.2 years (range, 36–68 years) and a mean body mass index of 24.3 kg/m^2 (range, 14.5–32.0 kg/m^2) participated in the study. These patients continuously received an oral dose of 750 mg of apatinib mesylate tablets (corresponding to 604 mg of apatinib free base) once daily for 28 days. Blood samples (2–3 ml) for metabolism and pharmacokinetic analyses were collected in heparinized tubes at 0 (predose), 0.5, 1, 2, 3, 4, 6, 8, 12, and 24 hours (before the next dose) on days 1 and 28, as well as 48 hours after the last dosing. Samples were centrifuged at 1000*g* for 10 minutes to separate the plasma fractions. The plasma samples were stored at −20°C until analysis.

Metabolite Profiling and Identification

Sample Preparation. Representative pooled human plasma, urine, and fecal homogenate samples were prepared for metabolite profiling. Equal volumes of plasma samples collected from all cancer patients at 0 hour (predose) and 4 and 8 hours after the last dosing were pooled by time point. Excreta (urine and fecal homogenates) samples from all healthy subjects were pooled in proportion to the total sample weight over 24-hour intervals. For every 200-μl aliquot of pooled plasma, urine, and fecal homogenate samples, 400 μl of acetonitrile was added. After vortex-mixing and centrifugation at 11,000*g* for 5 minutes, the supernatants were evaporated to dryness under a stream of nitrogen at 40°C. The residues were then reconstituted in 100 μl of acetonitrile-water (1:9). Reconstituted extract of pooled urine and fecal homogenate samples were diluted at ratios of 1:4 and 1:40, respectively, with acetonitrile-water (1:9) before analysis to achieve proper mass response. A 3-μl aliquot of the resulting solution was injected for metabolite identification.

UPLC-UV/Q-TOF MS Analysis. The LC separation of the metabolites was performed on an Acquity UPLC system (Waters Corporation, Milford, MA) using an Acquity UPLC HSS T3 column (100 mm × 2.1 mm, 1.8-μm particle size; Waters Corporation). The column temperature was set to 40°C, and the flow rate was kept to 450 μl/min. The mobile phase consisted of solvent A (5 mM ammonium acetate solution with 0.05% formic acid) and solvent B (acetonitrile), and a gradient method was used. The mobile phase was initially

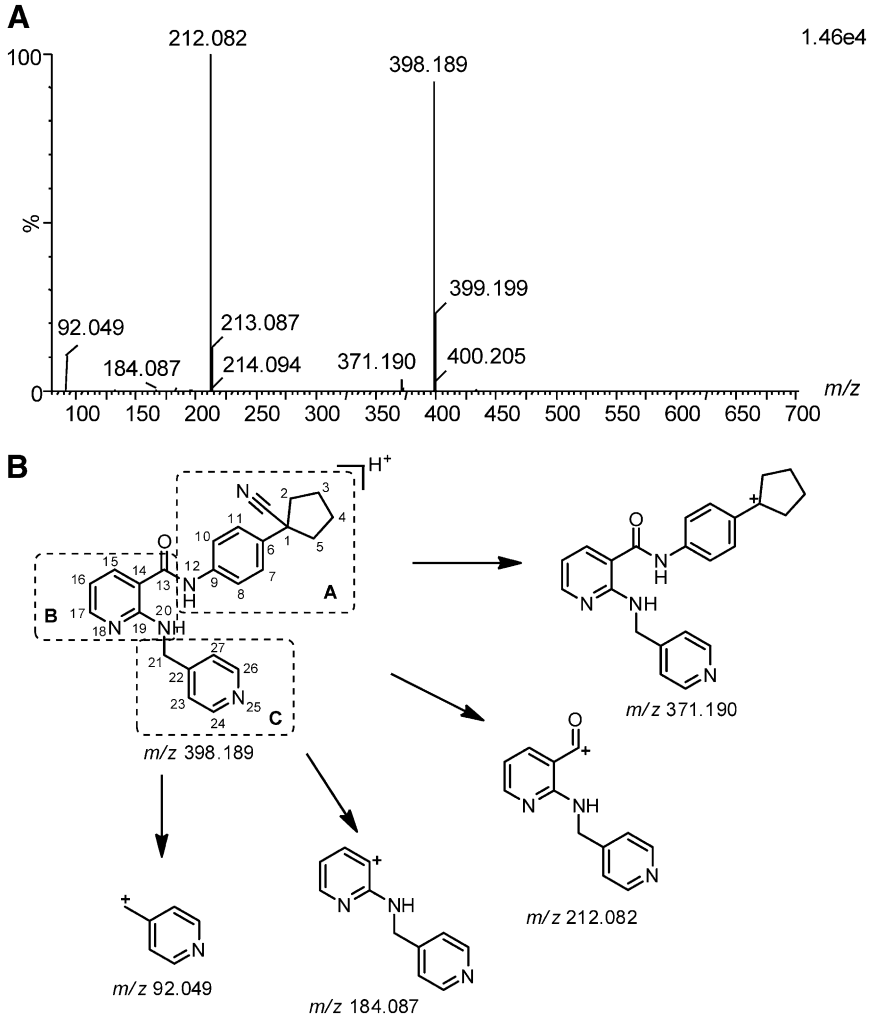

Fig. 1. Mass spectrum of apatinib at high collision energy (A) and the tentative structures of the most informative fragment ions for apatinib (B). The structure of apatinib could be divided into three parts (A, B, and C) based on the fragmentation pattern.

composed of solvent A/solvent B (95:5) and held for 2 minutes, then linearly programmed to solvent A/solvent B (40:60) over 13 minutes, and held for 1 minute and to solvent B (100%) for 1 minute. The mobile-phase condition was returned to the starting solvent mixture and allowed to equilibrate for 3 minutes before the next injection. The effluent was monitored using a UV detector at 340 nm.

Mass spectrometry was performed using a Synapt Q-TOF high-resolution mass spectrometer (Waters Corporation) operating in positive ion electrospray mode. Nitrogen and argon were used as desolvation and collision gases, respectively. The capillary and cone voltages were set to 3.5 kV and 50 V, respectively. The desolvation gas was set to 700 l/h at a temperature of 350°C. The source temperature was set to 100°C. The scan range was set at *m/z* (mass-to-charge ratio) 80−1000. All analyses were acquired using Lock Spray to ensure accuracy and reproducibility. Leucine-enkephalin (*m/z* 556.2771) at a concentration of 400 ng/ml and a flow rate of 3 μl/min was used for the lock mass. Data were collected in centroid mode. Data acquisition was performed using an alternating low and elevated collision energy (CE) scan mode, which allowed for the simultaneous acquisition of molecular ion and fragmentation ion data for all detected analytes within a single experiment. At low CE, the transfer and trap CEs were 2 and 4 eV, respectively. At high CE, the transfer CE was 15 eV and trap CE ramped from 5 to 25 eV.

Instrument control and postacquisition analyses were performed using a MetaboLynx (v4.1) program (Waters Corporation), which uses mass defect filtering and the dealkylation tool to generate a series of extracted ion chromatograms (XICs). The XICs correspond to the ion currents that fall within a 40-mDa window around the *m/z* values of the expected metabolites. The XICs of the control and samples were compared to eliminate the chromatographic peaks in the samples that also appear in the control (Zhang et al., 2008). Fragmentations were proposed using the Mass Frontier 7.0 software (Thermo Fisher Scientific Inc., San Jose, CA).

Enzyme Hydrolysis. Pooled human plasma and urine samples were adjusted to pH 5 using citrate buffer and treated with 2000 units of β-glucuronidase. The mixture was incubated in a water bath at 37°C for 16 hours; then the mixtures were treated as described already and analyzed. Incubated plasma and urine samples without the enzyme served as controls.

Reduction of *N*-Oxide Metabolites with Titanium Trichloride (TiCl3). To identify *N*-oxides, the pooled human plasma and urine samples were treated with $TiCl_3$, which can selectively reduce *N*-oxides to their corresponding amines (Kulanthaivel et al., 2004). $TiCl_3$ solution (20 μl) was added to a 200-μl aliquot of plasma and urine. The mixtures were kept on ice for 2 hours and neutralized with potassium hydroxide. Then the reaction mixtures were treated as described previously herein and analyzed.

Synthesis of Apatinib-25-*N*-Oxide. A solution of apatinib mesylate (100 mg in 1 ml of methanol) was added to a solution of m-chloroperbenzoic acid (100 mg in 20 ml of dichloromethane) and stirred at room temperature for 24 hours (Chelucci et al., 2008). The mixture was evaporated, and the residue was further purified using a Shimadzu LC-6AD semipreparative HPLC apparatus equipped with a SPD-20A UV detector. Separation was achieved using a YMC-Pack ODS-A column (10 × 250 mm I.D., 5 μm; YMC Company Ltd., Kyoto, Japan). The column oven was set to room temperature. Elution was performed using methanol-water (70:30, v/v) at a flow rate of 3 ml/min. The detection wavelength was set to 340 nm. The eluate at 9.8 minutes was collected and evaporated to obtain the synthetic standard of M1-6 (70% yield).

Preparation of the Major Metabolites from Human Urine. Pooled bulk urine samples were precipitated with methanol and concentrated to dryness. The residue was dissolved in 50 ml of anhydrous methanol-water (1:9) and

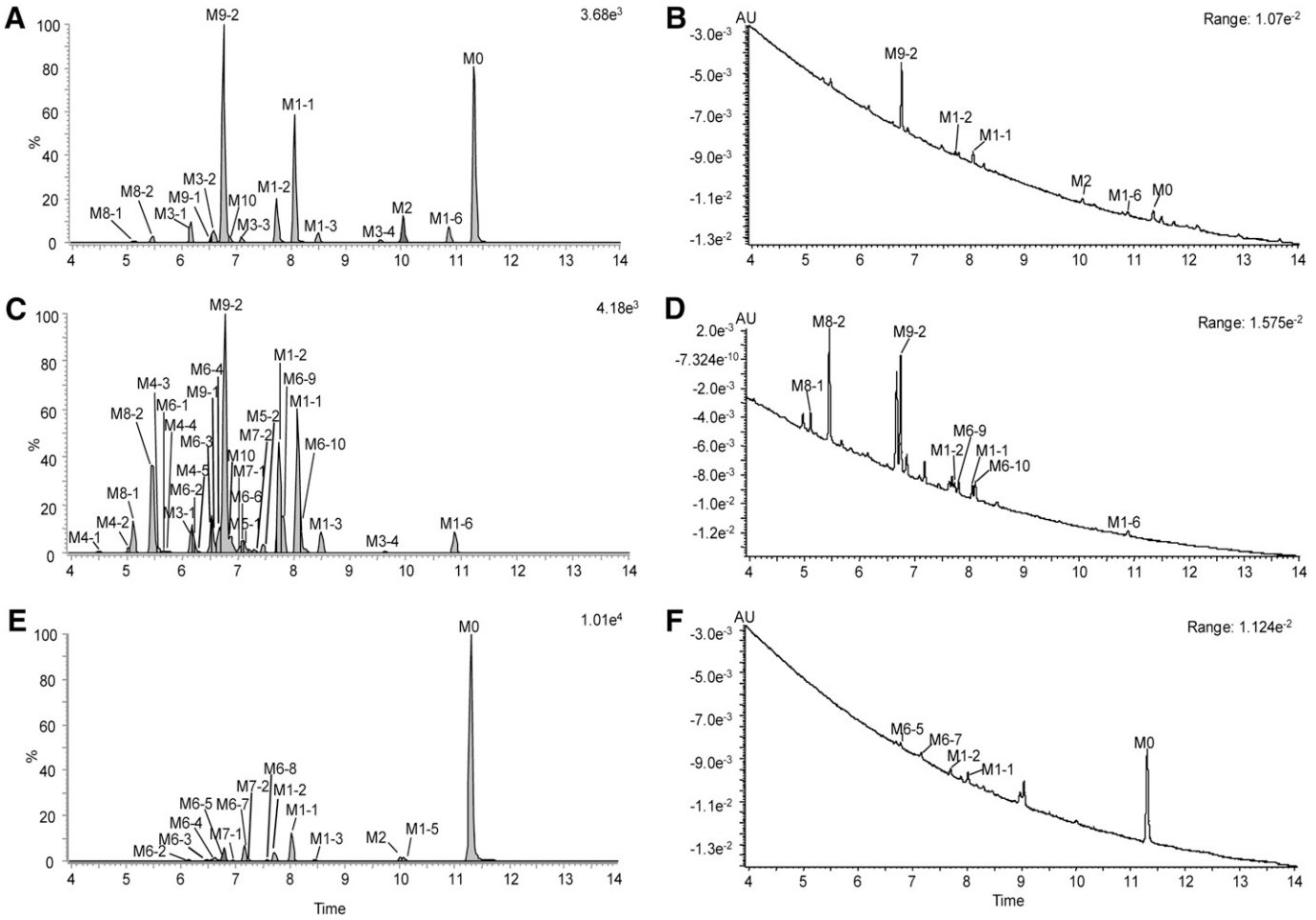

Fig. 2. Metabolic profiles of apatinib after oral administration of 750 mg of apatinib mesylate to humans. (A) MDF (mass defect filter) metabolic profile of pooled plasma samples collected 8 hours postdose at steady state; (B) UPLC-UV chromatogram of pooled plasma samples collected 8 hours postdose at steady state; (C) MDF metabolic profile of 0- to 24-hour pooled urine samples; and (D) UPLC-UV chromatogram of pooled 0- to 24-hour urine samples; (E) MDF metabolic profile of 24- to 48-hour pooled fecal samples; and (F) UPLC-UV chromatogram of pooled 24- to 48-hour fecal samples.

fractionated using YMC*GEL ODS-A-HG column chromatography (10%–100% anhydrous methanol), yielding seven fractions (A–G). Fraction D eluted by methanol-water (4:6) and fraction E eluted by methanol-water (5:5) were further purified on a Shimadzu LC-6AD semipreparative HPLC apparatus equipped with an SPD-20A UV detector. Chromatographic separation was achieved using a YMC-Pack ODS-A column (10 × 250 mm internal diameter, 5 μm; YMC Company Ltd.). The mobile phase consisted of solvent A (water with 0.1% formic acid) and solvent B (methanol), and a gradient method was used. The detection wavelength was set to 340 nm. Fraction D afforded M8-2 (26 mg), and fraction E afforded M4-7 (3 mg), M6-9 (8 mg), M6-10 (15 mg), and M9-2 (28 mg).

Quantification of Apatinib and Its Major Metabolites in Human Plasma

Apatinib, M1-1, M1-2, M1-6, and M9-2 were simultaneously determined using a previously reported LC-MS/MS method (Ding et al., 2012). M9-1 was also semiquantified using M9-2 as the calibration standard.

Pharmacokinetic Analysis

Standard noncompartmental methods were used to determine the pharmacokinetic parameters of apatinib and its metabolites using WinNonlin (Version 5.3; Pharsight, Mountain View, CA). The peak plasma concentration (C_{max}) and time to reach C_{max} (T_{max}) were taken directly from the pharmacokinetic concentration-time data. The elimination rate constant (k_e) value was estimated using least-squares regression of the terminal log-linear phase of the concentration-time curve, and the elimination half-life was calculated as $\ln 2/k_e$. The area under the plasma concentration-time curve ($AUC_{0-24\ hour}$) was calculated using the linear-log trapezoidal method. The accumulation ratios (day 28/day 1) for $AUC_{0-24\ hour}$ and C_{max} were also calculated.

Quantification of Apatinib and Its Major Metabolites in Human Urine and Feces

The concentrations of apatinib and its metabolites M1-1, M1-2, M1-6, M4-7, M6-9, M6-10, M8-2, and M9-2 in urine samples, as well as apatinib and its metabolites M1-1, M1-2, M1-6, and M6-9 (for the semiquantification of total dioxygenated metabolites) in fecal samples, were determined using the LC-MS/MS method. This method was partially validated, including selectivity, linearity, intraday precision and accuracy, matrix effect, recovery, and stability.

The preparation procedures for the urine samples were similar to those for the plasma except the resulting solution was diluted 10-fold with mobile phase before analysis. To a 10-μl aliquot of fecal homogenous, 960 μl of internal standard solution (500 ng/ml vatalanib) was added, and the mixture was thoroughly vortex-mixed. A 20-μl aliquot of the resulting solution was mixed with 180 μl of mobile phase before analysis. The LC-MS/MS analytical conditions for urine and fecal sample analysis were similar to those for plasma except more reaction monitoring transitions were selected: *m/z* 339–137 for M4-7, *m/z* 430 to (212 + 108) for M6-9 and M6-10, and *m/z* 499–323 for M8-2 were added for urine analysis; *m/z* 430–430 for M6-9 was added for fecal sample analysis. For urine sample analysis, the method was linear over the concentration range of 30.0–10,000 ng/ml for each analyte. For fecal sample analysis, the method was linear over the concentration ranges of 2.50–2000, 0.500–400, 0.250–200, 0.250–200, and 2.50–200 μg/g

TABLE 1

Identification of apatinib metabolites in human plasma, urine, and feces after oral administration of 750 mg of apatinib mesylate tablets using ultraperformance liquid chromatography-UV/quadrupole time-of-flight mass spectrometry

Name	Metabolic Pathway	*m/z* $[M + H]^+$	Formula	Error (PPM)	Retention Time (min)	Relative Peak Area%				Fragment Ions
						Plasma		Urine 0–24h	Feces 24–48 h	
						4 h	8 h			
M0	Parent	398.197	$C_{24}H_{23}N_5O$	−3.7	11.4	41.4	27.8	n.d.	76.7	371.186, 212.075, 92.048
M1-1[a]	*E*-3-hydroxylation	414.184	$C_{24}H_{23}N_5O_2$	−22.4	8.1	19.2	17.8	14.6	7.43	387.190, 212.085, 184.091, 92.052
M1-2[a]	*Z*-3-hydroxylation	414.190	$C_{24}H_{23}N_5O_2$	−7.7	7.7	7.43	6.31	12.0	2.92	387.199, 212.088, 184.095, 92.054
M1-3	Mono-oxygenation	414.188	$C_{24}H_{23}N_5O_2$	−13.0	8.5	1.61	1.41	1.71	0.47	212.085, 92.051
M1-4	Mono-oxygenation	414.194	$C_{24}H_{23}N_5O_2$	3.0	8.6	0.13	n.d.	n.d.	n.d.	212.082
M1-5	Mono-oxygenation	414.195	$C_{24}H_{23}N_5O_2$	5.4	10.1	0.10	n.d.	n.d.	0.87	228.079, 92.050
M1-6[a]	25-*N*-oxidation	414.192	$C_{24}H_{23}N_5O_2$	−1.6	10.9	1.70	2.28	2.35	0.12	397.191, 228.078, 108.044
M2	*N*-dealkylation	307.157	$C_{18}H_{18}N_4O$	3.1	10.0	2.67	3.55	n.d.	1.05	121.039
M3-1	*Z*-3-hydroxylation and *N*-dealkylation	323.157	$C_{18}H_{18}N_4O_2$	20.6	6.2	1.51	2.85	2.26	n.d.	121.040
M3-2	*E*-3-hydroxylation and *N*-dealkylation	323.148	$C_{18}H_{18}N_4O_2$	−9.9	6.6	1.65	1.73	0.52	n.d.	121.038
M3-3	Mono-oxygenation and *N*-dealkylation	323.157	$C_{18}H_{18}N_4O_2$	19.0	7.1	0.40	0.74	0.17	n.d.	121.040
M3-4	Mono-oxygenation and *N*-dealkylation	323.157	$C_{18}H_{18}N_4O_2$	19.9	9.6	0.19	0.42	0.10	n.d.	137.035
M4-1	Dioxygenation and *N*-dealkylation	339.144	$C_{18}H_{18}N_4O_3$	−5.0	4.5	n.d.	n.d.	0.19	n.d.	121.038
M4-2	Dioxygenation and *N*-dealkylation	339.144	$C_{18}H_{18}N_4O_3$	−6.2	5.1	n.d.	n.d.	0.61	n.d.	121.039
M4-3	Dioxygenation and *N*-dealkylation	339.151	$C_{18}H_{18}N_4O_3$	16.6	5.6	n.d.	n.d.	0.28	n.d.	121.041
M4-4	Dioxygenation and *N*-dealkylation	339.155	$C_{18}H_{18}N_4O_3$	27.5	5.8	n.d.	n.d.	0.15	n.d.	121.044
M4-5	Dioxygenation and *N*-dealkylation	339.150	$C_{18}H_{18}N_4O_3$	13.3	6.2	n.d.	n.d.	0.41	n.d.	137.036
M4-6	Dioxygenation and *N*-dealkylation	339.142	$C_{18}H_{18}N_4O_3$	−9.7	6.6	n.d.	n.d.	0.54	n.d.	137.035
M4-7[a]	*Z*-3-hydroxylation, 16-hydroxylation and *N*-dealkylation	339.141	$C_{18}H_{18}N_4O_3$	−14.2	6.8	n.d.	n.d.	0.66	n.d.	137.031
M4-8[a]	*E*-3-hydroxylation, 16-hydroxylation and *N*-dealkylation	339.148	$C_{18}H_{18}N_4O_3$	5.9	7.2	n.d.	n.d.	0.41	n.d.	137.034
M4-9	Dioxygenation and *N*-dealkylation	339.153	$C_{18}H_{18}N_4O_3$	21.6	7.7	n.d.	n.d.	0.17	n.d.	137.040
M5-1	Mono-oxyenation and dehydrogenation	412.180	$C_{24}H_{21}N_5O_2$	5.8	7.1	n.d.	n.d.	0.65	n.d.	210.072, 121.040
M5-2	Mono-oxyenation and dehydrogenation	412.185	$C_{24}H_{21}N_5O_2$	18.9	7.4	n.d.	n.d.	0.82	n.d.	210.068
M5-3	Mono-oxyenation and dehydrogenation	412.181	$C_{24}H_{21}N_5O_2$	8.2	7.8	0.15	n.d.	0.19	n.d.	108.043
M5-4	Mono-oxyenation and dehydrogenation	412.177	$C_{24}H_{21}N_5O_2$	0.2	8.6	0.08	n.d.	n.d.	n.d.	212.085
M6-1	Dioxygenation	430.195	$C_{24}H_{23}N_5O_3$	16.1	5.7	n.d.	n.d.	0.28	n.d.	212.088
M6-2	Dioxygenation	430.197	$C_{24}H_{23}N_5O_3$	20.5	6.2	n.d.	n.d.	1.36	0.31	212.085
M6-3	Dioxygenation	430.185	$C_{24}H_{23}N_5O_3$	−7.2	6.5	0.17	0.18	2.97	0.32	212.036
M6-4	Dioxygenation	430.178	$C_{24}H_{23}N_5O_3$	−22.3	6.7	0.18	0.20	2.71	0.99	212.038
M6-5	Dioxygenation	430.195	$C_{24}H_{23}N_5O_3$	15.4	6.8	n.d.	n.d.	n.d.	3.64	228.088, 92.053
M6-6	Dioxygenation	430.189	$C_{24}H_{23}N_5O_3$	3.5	7.1	n.d.	n.d.	0.91	n.d.	212.083
M6-7	Dioxygenation	430.195	$C_{24}H_{23}N_5O_3$	16.3	7.2	n.d.	n.d.	n.d.	4.42	228.089, 92.056
M6-8	Dioxygenation	430.202	$C_{24}H_{23}N_5O_3$	33.1	7.6	n.d.	n.d.	n.d.	0.26	228.091, 92.058
M6-9[a]	*Z*-3-hydroxylation and 25-*N*-oxidation	430.188	$C_{24}H_{23}N_5O_3$	−0.2	7.8	0.17	0.22	2.97	n.d.	212.036, 108.020
M6-10[a]	*E*-3-hydroxylation and 25-*N*-oxidation	430.180	$C_{24}H_{23}N_5O_3$	−18.2	8.1	0.20	0.39	5.21	n.d.	212.027, 108.037
M6-11	Dioxygenation	430.185	$C_{24}H_{23}N_5O_3$	−6.5	8.5	n.d.	n.d.	0.67	n.d.	212.082, 108.043
M7-1	Mono-oxygenation and sulfation	494.151	$C_{24}H_{23}N_5O_5S$	2.2	7.0	n.d.	n.d.	0.21	0.15	212.081
M7-2	Mono-oxygenation and sulfation	494.150	$C_{24}H_{23}N_5O_5S$	1.0	7.3	0.08	n.d.	0.43	0.33	212.086
M8-1	*Z*-3-hydroxylation, *N*-dealkylation and *O*-glucuronidation	499.174	$C_{24}H_{26}N_4O_8$	−17.8	5.1	n.d.	0.16	3.01	n.d.	323.151, 121.038
M8-2[a]	*E*-3-hydroxylation, *N*-dealkylation and *O*-glucuronidation	499.181	$C_{24}H_{26}N_4O_8$	−3.7	5.5	0.52	0.82	10.3	n.d.	323.151, 121.038
M9-1	*Z*-3-hydroxylation and *O*-glucuronidation	590.220	$C_{30}H_{31}N_5O_8$	−9.1	6.5	0.69	0.53	1.07	n.d.	414.195, 212.082
M9-2[a]	*E*-3-hydroxylation and *O*-glucuronidation	590.213	$C_{30}H_{31}N_5O_8$	−20.3	6.8	19.6	32.2	27.9	n.d.	414.183, 212.079, 92.047
M10	Dioxygenation and glucuronidation	606.210	$C_{30}H_{31}N_5O_9$	−16.0	6.9	0.20	0.44	1.30	n.d.	430.183, 108.042

n.d., not detected; PPM, parts per million.

[a]Metabolites that were confirmed by comparison with reference standards after cochromatography, mass spectrometry, and NMR.

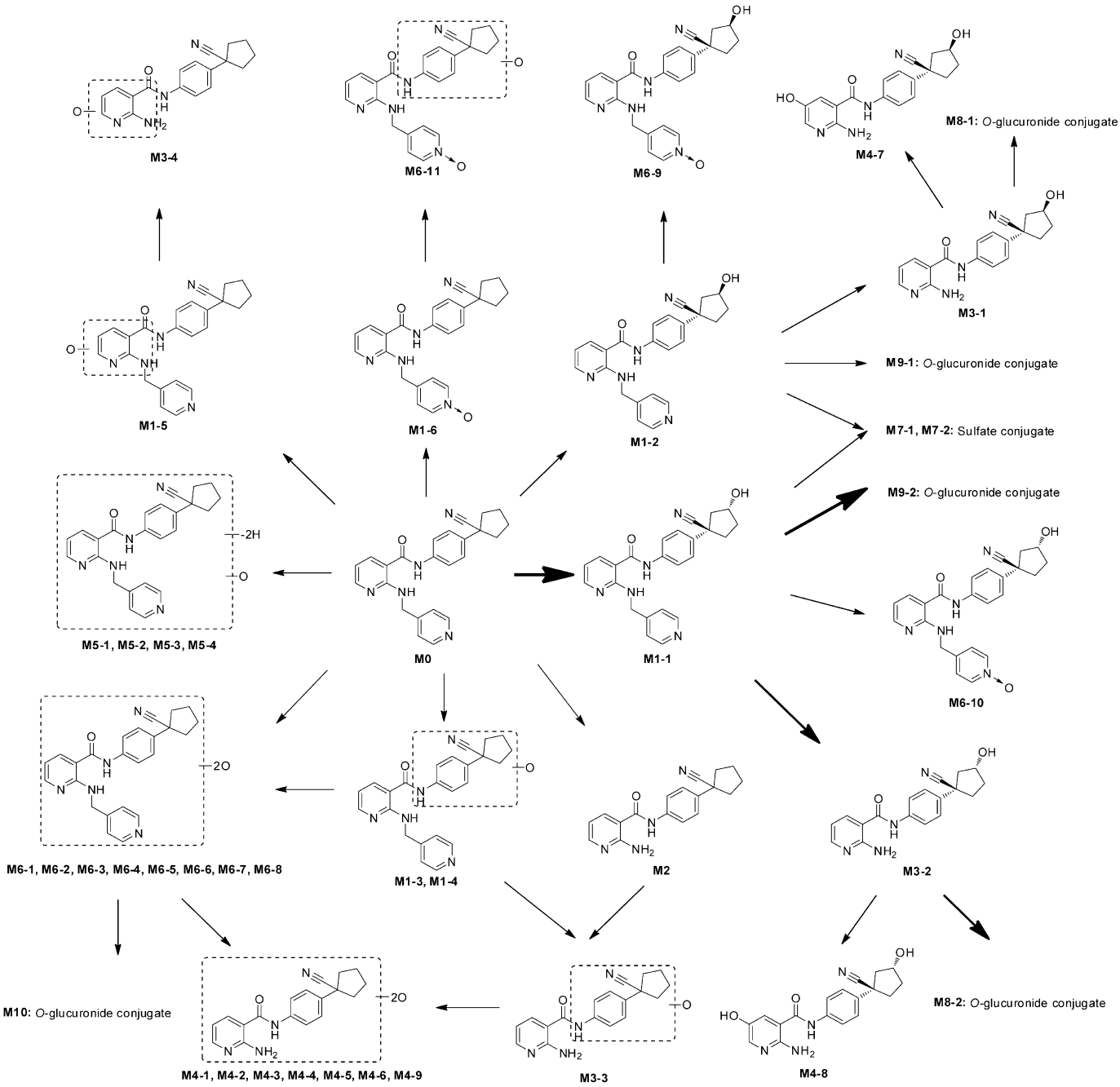

Fig. 3. Proposed metabolic pathways of apatinib in humans.

for apatinib, M1-1, M1-2, M1-6, and M6-9, respectively. The amount of apatinib and its major metabolites excreted in urine and feces during each collection interval was calculated by multiplying the concentration of each analyte by the volume or weight of the matrix collected over that interval. The total urinary recovery or fecal recovery was calculated as the cumulative amount excreted over all the collection periods and expressed as a percentage of the administered dose.

Binding of Apatinib and Its Major Metabolites to Human Plasma Proteins

The binding of apatinib, M1-1, M1-2, and M1-6 to human plasma proteins was measured by ultracentrifugation with similar methods as described previously (Verbeke et al., 1979). Triplicate samples of apatinib, M1-1, M1-2, and M1-6 at concentrations in the range of therapeutic plasma levels (500 ng/ml for apatinib; 50 ng/ml for M1-1, M1-2, and M1-6) were tested, and data are presented as mean ± standard deviation.

In Vitro Pharmacological Activity of Major Metabolites

Metabolites M1-1, M1-2, M1-6, and M9-2 were screened for their activity toward the inhibition of VEFGR-2, PDGFR-β, and c-kit RTKs using a previously reported assay format (Hunt et al., 2004). For comparison, the pharmacological activity of apatinib was also evaluated under the same conditions. A pharmacological activity index (PAI) was calculated by dividing the unbound concentration/in vitro potency ratio of each major metabolite by the corresponding ratio of the parent drug to quantify the contribution of each major metabolite to the overall effect of the drug (Leclercq et al., 2009). As described previously, a PAI value greater than 25% means the metabolite may

TABLE 2

^{1}H NMR data of apatinib (M0), *E*-3-hydroxy-apatinib (M1-1), *Z*-3-hydroxy-apatinib (M1-2), apatinib-25-*N*-oxide (M1-6), *Z*-3-hydroxy-16-hydroxy-*N*-dealkylated metabolite (M4-7), *E*-3-hydroxy-16-hydroxy-*N*-dealkylated metabolite (M4-8), *Z*-3-hydroxy-25-*N*-oxide metabolite (M6-9), *E*-3-hydroxy-25-*N*-oxide metabolite (M6-10), *E*-3-hydroxy-*O*-glucuronide-*N*-dealkylated metabolite (M8-2), and *E*-3-hydroxy-apatinib-*O*-glucuronide (M9-2).

Position	δH(J/Hz)									
	Apatinib[a]	M1-1[a]	M1-2[a]	M1-6[b]	M4-7[b]	M4-8[b]	M6-9[b]	M6-10[b]	M8-2[b]	M9-2[b]
H-2,4,5	2.40 (m, 2H)	2.73 (dd,J = 13.5, 6.0, 1H)	2.53 (m, 1H)	2.42 (m, 2H)	2.62(m, 1H)	2.82 (dd,J = 14.0, 6.0,1H)	2.64(m,1H)	2.82 (dd,J=14.0,6.4,1H)	2.75 (dd,J=14.8,6.8,1H)	2.87 (dd,J=14.8,6.4,1H)
	2.05 (m, 2H)	1.98 (dd,J = 13.5, 6.0, 1H)	2.31 (m, 2H)	2.12 (m, 2H)	2.43(m, 2H)	2.11 (dd,J = 14.0, 6.0,1H)	2.43(m,2H)	2.12 (dd,J=14.0,6.4,1H)	2.37(m,3H)	2.39(m,3H)
	1.88 (m, 4H)	2.36 (m,1H),1.97 (m, 1H)	2.09 (m, 2H)	1.98 (m, 4H)	2.21(m, 2H)	2.36 (m,3H)	2.22(m,2H)	2.37(m,2H)	2.20(m,2H)	2.19(m,2H)
		2.23 (m,1H), 2.04 (m, 1H)	1.80 (m, 1H)		1.96(m, 1H)	1.95 (m,1H)	1.97(m,1H)	2.22(m,2H)		
H-3		4.41 (m,1H)	4.37 (m, 1H)		4.51(m, 1H)	4.57 (m,1H)	4.52(m,1H)	4.57(m,1H)	4.65(m,1H)	4.64(m,1H)
H-7,11	7.49 (d,J = 8.7, 2H)	7.49 (d,J = 8.8, 2H)	7.46 (d,J = 8.5, 2H)	7.48 (d,J = 8.6, 2H)	7.43 (d,J = 8.7, 2H)	7.51 (d,J = 8.8, 2H)	7.47(d,J=8.4,2H)	7.52 (m,overlapped,2H)	7.56(d,J=8.8,2H)	7.55(d,J=8.4,2H)
H-8, 10	7.78 (d,J = 8.7, 2H)	7.75 (d,J = 8.8, 2H)	7.75 (d,J = 8.5, 2H)	7.73 (d,J = 8.6, 2H)	7.62 (d,J = 8.7, 2H)	7.63 (d,J = 8.8, 2H)	7.73(d,J=8.4,2H)	7.73(d,J=8.4,2H)	7.70(d,J=8.8,2H)	7.72(d,J=8.4,2H)
H-15	8.15 (dd,J = 7.7, 1.4, 1H)	8.09 (dd,J = 7.5, 2.0, 1H)	8.08 (dd,J = 7.5, 2.0, 1H)	8.05 (dd,J = 7.8, 1.5, 1H)	5.72 (d,J = 9.5, 1H)	5.73 (d,J = 9.6, 1H)	8.05 (dd,J=7.6,1.6,1H)	8.06 (dd,J=7.6,1.2,1H)	8.11(m,1H)	8.09(m,1H)
H-16	6.74 (dd,J = 7.7, 5.0, 1H)	6.68 (dd,J = 7.5, 5.0, 1H)	6.68 (dd,J = 7.5, 5.0, 1H)	6.69 (dd,J = 7.8, 4.9, 1H)			6.70 (dd,J=7.6,4.8,1H)	6.70 (dd,J=7.6,4.8,1H)	6.75 (dd,J=7.6,5.2,1H)	6.70 (dd,J=7.6,5.2,1H)
H-17	8.10 (dd,J = 5.0, 1.4, 1H)	8.14 (dd,J = 5.0, 2.0, 1H)	8.14 (dd,J = 5.0, 2.0, 1H)	8.10 (dd,J = 4.9, 1.5, 1H)	7.98 (d,J = 9.5, 1H)	7.98 (d,J = 9.6, 1H)	8.12 (dd,J=4.8,1.6,1H)	8.12 (dd,J=4.8,1.2,1H)	8.08(m,1H)	8.07(m,1H)
H-21	4.90 (d,J = 5.4, 2H)	4.67 (d,J = 5.9, 2H)	4.68 (d,J = 5.0, 2H)	4.74 (s, 2H)			4.75(s,2H)	4.75(s,2H)		4.80(s,2H)
H-23,27	7.90 (d,J = 6.0, 2H)	7.27 (d,J = 6.0, 2H)	7.28 (d,J = 6.0, 2H)	7.50 (d,J = 7.0, 2H)			7.52(d,J=6.4,2H)	7.54 (m,overlapped,2H)		7.50(d,J=5.6,2H)
H-24,26	8.78 (d,J = 6.0, 2H)	8.45 (d,J = 6.0, 2H)	8.44 (d,J = 6.0, 2H)	8.24 (d,J = 7.0, 2H)			8.24(d,J=6.4,2H)	8.24(d,J=6.4,2H)		8.46(d,J=5.6,2H)
H-1′									4.45(d,J=8.0,1H)	4.45(d,J=7.6,1H)
H-2′									3.41(t,J=9.2,1H)	3.41(t,J=9.2,1H)
H-3′									3.52(t,J=9.2,1H)	3.52(t,J=9.2,1H)
H-4′									3.23(t,J=9.2,1H)	3.23(t,J=9.2,1H)
H-5′									3.80(d,J=9.6,1H)	3.81 (d,J=10.0,1H)

[a] Dimethylsulfoxide (DMSO)-D_6, 500 MHz.
[b] CD_3OD (deuterated methanol), 400 MHz.

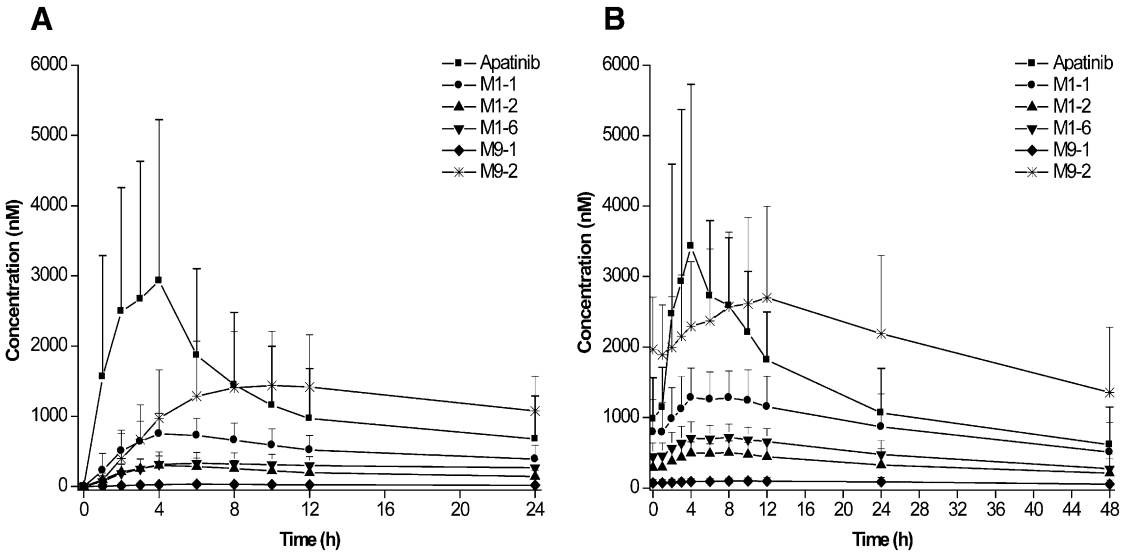

Fig. 4. Mean plasma concentration-time profiles of apatinib, M1-1, M1-2, M1-6, M9-1, and M9-2 after oral administration of 750 mg apatinib mesylate once daily for 28 day to 20 patients with advance colorectal cancer on days 1 (A) and 28 (B).

make a significant contribution to the effect of the drug activity (Smith and Obach, 2005).

Oxidative Metabolism of Apatinib in Microsomes and Recombinant P450 and FMO Isoforms

Recombinant human CYP enzymes (CYP1A2, 1B1, 2A6, 2B6, 2C8, 2C9, 2C19, 2D6, 2E1, 3A4, 3A5, and 4A11) or FMO enzymes (FMO1, FMO2, and FMO3) or microsomes (HLMs, HIMs, HPMs, and HRMs) were incubated with apatinib. The incubation mixtures (200 μl) contained phosphate buffer (100 mM, pH 7.4), P450 (50 pmol P450/ml) or FMO (0.25 mg protein/ml) or microsomes (1 mg protein/ml), apatinib (2 μM), and NADPH (2 mM). After 1-hour incubation at 37°C, ice-cold acetonitrile (200 μl) was added to each incubation to stop the reaction. Incubations were performed in duplicate and analyzed by LC-MS/MS and UPLC-UV/Q-TOF MS.

HLM Incubations in the Presence of Selective P450 Inhibitors

The duration of incubation and the protein concentrations used above were useful for initial experiments aimed at the identification of metabolites in microsomal incubations, but they might not represent linear conditions. To determine conditions that are linear for time of incubation and protein concentration, 2 μM apatinib was incubated in HLMs (0–1.0 mg protein/ml) or P450 enzymes (0–50 pmol P450/ml, CYP3A4, CYP3A5, or CYP2D6) with 2 mM NADPH at 37°C across a range of incubation times (0–90 minutes). Based on the results obtained, a 10-minute incubation and a final HLM concentration of 0.2 mg protein/ml and P450 enzyme concentration of 10 pmol P450/ml represented conditions that are linear and were used in the subsequent experiments.

The incubation mixtures (200 μl in duplicate) contained phosphate buffer (100 mM, pH 7.4), HLM (0.2 mg protein/ml), apatinib (2 μM), NADPH (1 mM), and a single selective P450 inhibitor. The chemical inhibitors used were α-naphthoflavone (1 μM) for CYP1A1/2, sulfaphenazole (6 μM) for CYP2C9, ticlopidine (10 μM) for CYP2B6 and CYP2C19, quinidine (2 μM) for CYP2D6, ketoconazole (1 μM) for CYP3A4/5, chlormethiazole (24 μM) for CYP2E1, and ABT (1 mM) for all the P450s. Metabolism-dependent inhibitor ticlopidine was preincubated with HLM in the presence of NADPH for 10 minutes before the substrate was added. After the substrate addition, the samples were then incubated at 37°C for 10 minutes. Reactions were terminated by the addition of an equal volume of ice-cold acetonitrile. The formations of M1-1, M1-2, M1-3, M1-5, M1-6, M2, and M3-1 in the presence of inhibitors were compared with metabolites formed in their absence.

To provide additional evidence for the contribution of FMOs to the formation of M1-6 (pridine *N*-oxide), HLMs were heat-treated at 45°C for 5 minutes before incubation with apatinib. These treatment conditions would be expected to inactivate the heat-sensitive FMOs but do not appreciably affect P450 enzyme activities (Tugnait et al., 1997). Incubation conditions and sample preparation were similar as described already herein.

Formation of M1-1, M1-2, and M1-6 by Recombinant P450 and FMO Isoforms

To probe further the specific isoforms involved in the formation of major oxidative metabolites (M1-1, M1-2, and M1-6), 2 μM apatinib was incubated

TABLE 3

Pharmacokinetic parameters (mean ± S.D.) of apatinib and its major metabolites in human plasma after oral administration of 750 mg of apatinib mesylate once daily for 28 days to 20 patients with advanced colorectal cancer

Time	Parameter	Apatinib	M1-1	M1-2	M1-6	M9-1	M9-2
Day 1	T_{max} (h)	2.9 ± 1.4	5.2 ± 4.8	5.0 ± 4.8	7.7 ± 6.3	7.1 ± 4.5	10.2 ± 3.7
	C_{max} (nmol/l)	3819 ± 2204	849 ± 268	339 ± 131	375 ± 172	36.5 ± 22.0	1543 ± 819
	$AUC_{0-24\ h}$ (nmol·h/l)	30,941 ± 18,794	12,458 ± 4380	4796 ± 2049	6605 ± 2806	555 ± 322	27,276 ± 14,147
Day 28	T_{max} (h)	4.7 ± 2.2	7.2 ± 6.2	7.0 ± 6.1	5.5 ± 2.4	11.5 ± 8.0	11.3 ± 6.9
	C_{max} (nmol/l)	3935 ± 2211	1470 ± 418	571 ± 162	786 ± 210	94.3 ± 55.5	2843 ± 1226
	$AUC_{0-24\ h}$ (nmol·h/l)	46,285 ± 17,883	26,014 ± 8895	10,001 ± 4107	14,596 ± 4090	2168 ± 1184	57,631 ± 24,888
	$t_{1/2}$ (h)	18.6 ± 9.2	24.7 ± 12.9	23.2 ± 12.3	21.2 ± 12.7	26.3 ± 15.9	23.8 ± 9.7
Day 28/day 1	C_{max} ratio	1.16 ± 0.82	1.78 ± 0.79	1.76 ± 0.97	2.41 ± 1.75	3.01 ± 2.15	1.84 ± 1.13
	$AUC_{0-24\ h}$ ratio	1.77 ± 1.17	2.18 ± 1.13	2.20 ± 1.38	2.51 ± 1.79	3.69 ± 2.95	2.17 ± 1.35

AUC, area under the curve; C_{max}, peak plasma concentration; $t_{1/2}$, elimination half-life; T_{max}, time to reach C_{max}.

TABLE 4

Excretion of total drug-related compounds in urine and feces after a single oral administration of 750 mg of apatinib mesylate tablets to 12 healthy subjects

Time Period (h)	%Dose Recovered by Subject														
	Male						Female						Mean ± S.D.		
	1	2	3	4	5	6	1	2	3	4	5	6	Total	Male	Female
Urine															
0–4	0.924	0.453	0.757	0.560	0.780	0.333	0.483	0.460	0.484	0.545	0.528	0.364	0.556 ± 0.177	0.635 ± 0.223	0.477 ± 0.064
0–8	2.42	1.04	2.02	1.60	1.90	0.705	0.873	1.51	1.33	2.10	1.25	1.45	1.52 ± 0.52	1.61 ± 0.64	1.42 ± 0.40
0–12	3.48	1.46	3.36	2.00	2.76	0.951	1.47	2.25	2.02	3.88	1.77	2.41	2.32 ± 0.90	2.33 ± 1.03	2.30 ± 0.85
0–24	5.56	2.58	5.07	3.04	4.84	1.68	3.56	4.36	3.30	6.60	2.65	4.28	3.96 ± 1.42	3.80 ± 1.57	4.13 ± 1.37
0–36	7.42	3.74	6.85	3.80	6.19	2.58	4.96	5.79	4.43	8.50	3.38	5.54	5.26 ± 1.78	5.10 ± 1.97	5.43 ± 1.73
0-48	8.12	4.22	7.77	4.37	6.90	3.29	5.80	6.75	5.34	9.28	3.98	6.02	5.99 ± 1.85	5.78 ± 2.06	6.20 ± 1.77
0–72	8.90	4.49	8.19	4.80	7.59	5.22	6.77	7.41	6.25	10.1	4.73	6.76	6.77 ± 1.78	6.53 ± 1.92	7.01 ± 1.78
0–96	9.06	4.63	8.25	4.86	7.76	5.67	7.46	7.63	6.56	10.4	4.98	7.04	7.02 ± 1.77	6.70 ± 1.89	7.34 ± 1.76
Feces															
0–24	5.10	35.1	30.9	NA	NA	NA	NA	NA	NA	NA	42.5	0.623	9.52 ± 16.3	11.9 ± 16.6	7.19 ± 17.3
0–48	5.10	81.3	55.2	82.0	24.4	NA	51.9	63.2	79.3	0.008	68.4	59.5	47.5 ± 31.8	41.3 ± 36.7	53.7 ± 27.9
0-72	66.6	81.3	55.2	94.7	54.0	NA	55.6	67.1	85.2	44.0	68.4	65.4	61.5 ± 24.1	58.6 ± 32.7	64.3 ± 13.8
0–96	72.5	95.3	55.9	96.6	58.5	55.3	62.0	68.7	87.6	46.3	71.0	67.9	69.8 ± 16.1	72.4 ± 19.3	67.3 ± 13.4
Urine + feces															
0–24	10.7	37.7	36.0	3.04	4.84	1.68	3.56	4.36	3.30	6.60	45.1	4.91	13.5 ± 16.0	15.6 ± 16.7	11.3 ± 16.6
0-48	13.2	85.5	63.0	86.4	31.3	3.29	57.7	70.0	84.6	9.29	72.4	65.5	53.5 ± 31.0	47.1 ± 36.3	59.9 ± 26.3
0-72	75.5	85.8	63.4	99.5	61.6	5.22	62.4	74.5	91.5	54.1	73.1	72.2	68.2 ± 23.8	65.2 ± 32.6	71.3 ± 12.6
0–96	81.6	99.9	64.2	101.5	66.3	61.0	69.5	76.3	94.2	56.7	76.0	74.9	76.8 ± 14.9	79.1 ± 18.2	74.6 ± 12.1

NA, not applicable.

with recombinant human CYP1A2, 1B1, 2A6, 2B6, 2C8, 2C9, 2C19, 2D6, 2E1, 3A4, 3A5, and 4A11 (10 pmol P450/ml) or FMO1, FMO2, and FMO3 (0.2 mg protein/ml) at 37°C for 10 minutes (final incubation volume 200 μl). The incubations were initiated by the addition of 1 mM NADPH and terminated by the addition of 200 μl of ice-cold acetonitrile. Incubations were conducted in duplicate and analyzed by LC-MS/MS.

In Vitro Enzyme Kinetic Study

Enzyme kinetic parameters for the formation of M1-1, M1-2, and M1-6 were evaluated in HLMs (0.2 mg of protein/ml) and recombinant CYP3A4, CYP3A5, and CYP2D6 enzymes (10 pmol P450/ml). Incubations were performed at 37°C for 10 minutes. The substrate concentration ranged from 0.1 to 15 μM. Data are presented as averages of triplicate experiments. Kinetic constants were obtained by fitting Michaelis-Menten equation ($V = V_{max} \times S/(K_m + S)$) to experimental data using nonlinear regression (Prism 5.0; GraphPad Software Inc., San Diego, CA). V is the reaction velocity, V_{max} is the maximum velocity, K_m is the Michaelis constant (substrate concentration at 0.5 V_{max}), and S is the substrate concentration. In vitro intrinsic clearance (CL_{int}) was calculated as V_{max}/K_m. The fitness of the model was investigated based on visual inspection of the Eadie-Hofstee plots (corresponding to V against V/S) and calculated correlation coefficient.

Phase 2 Microsomal Incubations

The protein content and time linearity were proven in the preceding analysis. M1-1 and M1-2 (20 μM) were incubated with HLMs, HIMs, HPMs, and HRMs (0.5 mg protein/ml in 100 mM Tris-HCl buffer containing 8 mM $MgCl_2$ and 25 μg/ml alamethicin, pH 7.5) at 37°C for 1 hour with or without 2 mM UDPGA in a total volume of 200 μl. After preincubation of the reaction mixtures for 5 minutes at 37°C, the reactions were initiated by the addition of UDPGA and terminated by the addition of 200 μl ice-cold acetonitrile. Incubations were performed in duplicate and analyzed by UPLC-UV/Q-TOF MS.

O-Glucuronidation of M1-1 and M1-2 by Recombinant UGT Isoforms

The enzymes involved in the *O*-glucuronidation of M1-1 and M1-2 were determined using a panel of recombinant human UGT enzymes, including UGT1A1, UGT1A3, UGT1A4, UGT1A6, UGT1A7, UGT1A8, UGT1A9, UGT1A10, UGT2B4, UGT2B7, UGT2B15, and UGT2B17. The concentration

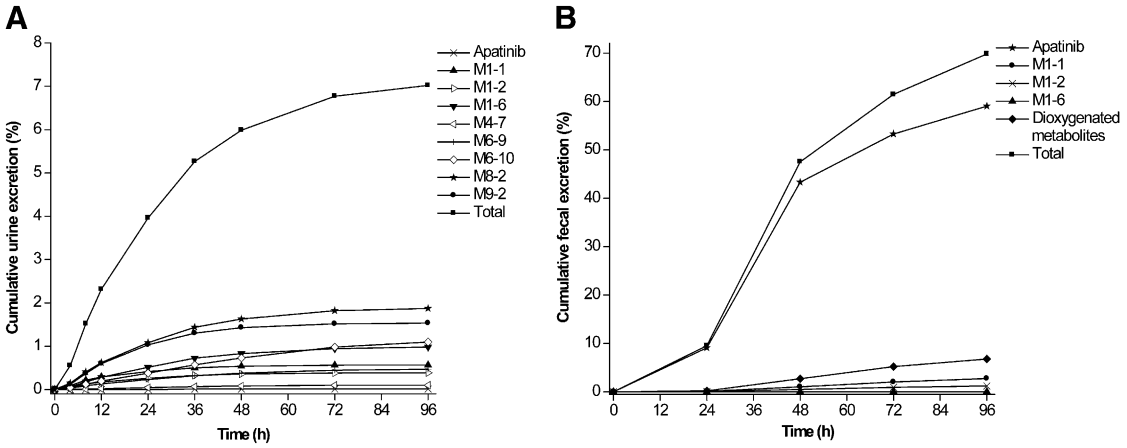

Fig. 5. Mean cumulative urine excretion (A) and fecal excretion (B) of apatinib and its major metabolites after a single oral administration of 750 mg of apatinib mesylate to 12 healthy Chinese volunteers.

TABLE 5

Binding of apatinb, M1-1, M1-2, and M1-6 to human plasma proteins and the in vitro pharmacological study results of M1-1, M1-2, M1-6, and M9-2

Group	Analyte	Percent Protein Binding[a]	IC_{50} (nM)			PAI (%)[b]		
			VEGFR-2	PDGFR-β	c-kit	VEGFR-2	PDGFR-β	c-kit
1	Apatinib	92.4 ± 3.2	1.90	16.5	12.9	100	100	100
	M1-1	90.1 ± 2.2	19.2	46.9	125	5.42	19.3	5.66
	M1-2	88.0 ± 3.2	179	1352	2511	0.22	0.25	0.11
2	Apatinib	92.4 ± 3.2	3.30	11.4	29.3	100	100	100
	M1-6	75.8 ± 3.7	265	369	981	0.32	0.80	0.77
	M9-2	Not measured	Inactive	Inactive	Inactive	Inactive	Inactive	Inactive

AUC, area under the curve; PAI, pharmacological activity index; PDGFR-β, platelet-derived growth factor receptor-β; VEGFR-2, vascular endothelial growth factor receptor-2.

[a] Percent protein binding was measure by ultracentrifugation.

[b] PAI was calculated as follows: PAI = (metabolite AUC at steady state × percent protein binding of metabolite × IC_{50} of parent)/(parent AUC at steady state × parent percent protein binding × IC_{50} of metabolite) × 100.

of the UGT enzymes was 0.5 mg of protein/ml. Incubations were performed in duplicate and analyzed by LC-MS/MS.

Inhibition of *O*-Glucuronidation of M1-1 and M1-2 by Selective UGT Inhibitors

Mefenamic acid (Mano et al., 2007a) and flurbiprofen (Mano et al., 2007b), two potent inhibitors of UGT2B7, as well as hecogenin (Uchaipichat et al., 2006), a potent inhibitor of UGT1A4, were tested for their inhibitory effect on the *O*-glucuronidation of M1-1 and M1-2 in HLMs. To determine the IC_{50} values of these inhibitors, M1-1 and M1-2 (20 μM) were incubated in the absence and presence of mefenamic acid (0.2–20 μM), racemic flurbiprofen (1–200 μM), or hecogenin (1–100 μM) in HLMs. Incubations were performed in duplicate and analyzed by LC-MS/MS.

Results

Metabolite Profiling and Identification. Metabolites of apatinib in human plasma, urine, and fecal samples were identified based on the generated elemental composition of ions obtained from accurate mass measurements, specific MS fragmentation pattern, and cochromatography (when standard available). The chromatographic and MS fragmentation behaviors of apatinib were first investigated to aid in the structural assignment of the metabolites. Apatinib had a retention time of 11.4 minutes on the HPLC system and showed a protonated molecule ion at *m/z* 398.189. The high CE mass spectrum (Fig. 1A) showed a major fragment ion at *m/z* 212.082, which was formed through cleavage of the nicotinamide amide bond and charge retention on the pyridyl moiety. The fragment ion at *m/z* 371.190 was formed through the cleavage of the cyano group. The fragment ion at *m/z* 184.087 represented the picolyl-aminopyridine moiety. The fragment ion at *m/z* 92.049 represented the picolyl group. Based on the MS fragment pattern, the structure of apatinib was divided into parts A, B, and C (Fig. 1B). The structures of the metabolites were then tentatively characterized by determining the changes in the *m/z* values of these three segments. The proposed MS fragmentation pattern of apatinib is shown in Fig. 1B.

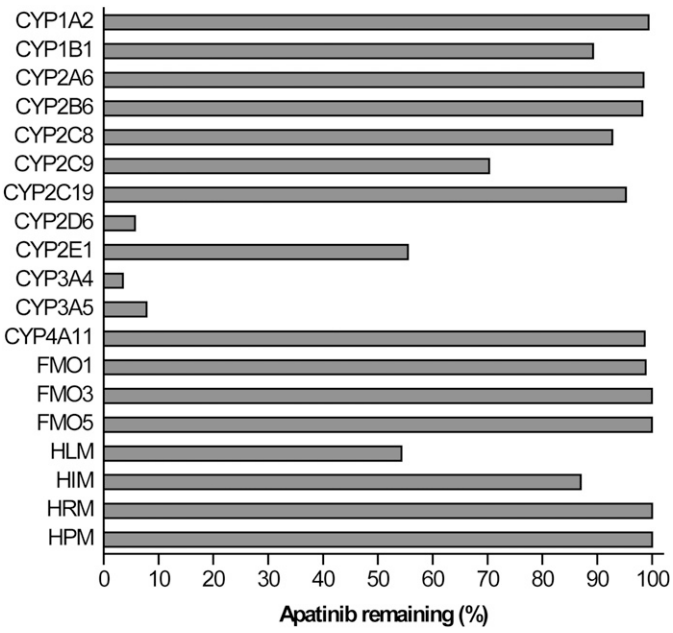

Fig. 6. Incubation of apatinib (2 μM) in recombinant human P450 and FMO enzymes and HLMs in the presence of 2 mM NADPH at 37°C for 1 hour. Each bar represents the mean of duplicate determinations.

After being processed using the mass defect filtering and dealkylation techniques, a total of 23, 35, and 14 metabolites of apatinib were detected in human plasma, urine, and feces, respectively (Fig. 2, A, C, and E). The corresponding UV chromatograms are shown in Fig. 2, B, D, and F, respectively. Based on the UV chromatograms, M9-2 was the major circulating drug-related component at steady state, followed by M0, M1-1, M1-6, and M1-2. The major components in urine included M1-1, M1-2, M6-9, M6-10, M8-2, and M9-2. M0 was the predominant component in feces, followed by M1-1, M6-7, M6-5, and M1-2. Table 1 lists the detailed information of the possible metabolites of apatinib, including protonated molecule ion, proposed elemental composition, retention time of each chromatographic peak, relative MS peak area, and the characteristic fragment ions. The proposed metabolic pathways of apatinib in humans are shown in Fig. 3. A description of the information used for the assignment of each metabolite is detailed in Supplemental Results. Nine major metabolites (M1-1, M1-2, M1-6, M4-7, M4-8, M6-9, M6-10, M8-2, and M9-2) were confirmed by comparison with reference standards. The ^{1}H NMR data of reference standards are listed in Table 2.

Pharmacokinetic Evaluation in Patients with Advanced Colorectal Cancer. The plasma concentration-time profiles of apatinib and its metabolites M1-1, M1-2, M1-6, M9-1, and M9-2 after oral administration of 750 mg of apatinib mesylate once daily for 28 day to patients with advanced colorectal cancer are shown in Fig. 4. A summary of their main pharmacokinetic parameters is presented in Table 3.

After the first dose, the C_{max} of apatinib, M1-1, M1-2, M1-6, M9-1, and M9-2 were achieved approximately 2.9 to 10.2 hour postdose, with mean values of 3819, 849, 339, 375, 36.5, and 1543 nmol/l, respectively. During the first 24 hours after dosing, the systemic exposures

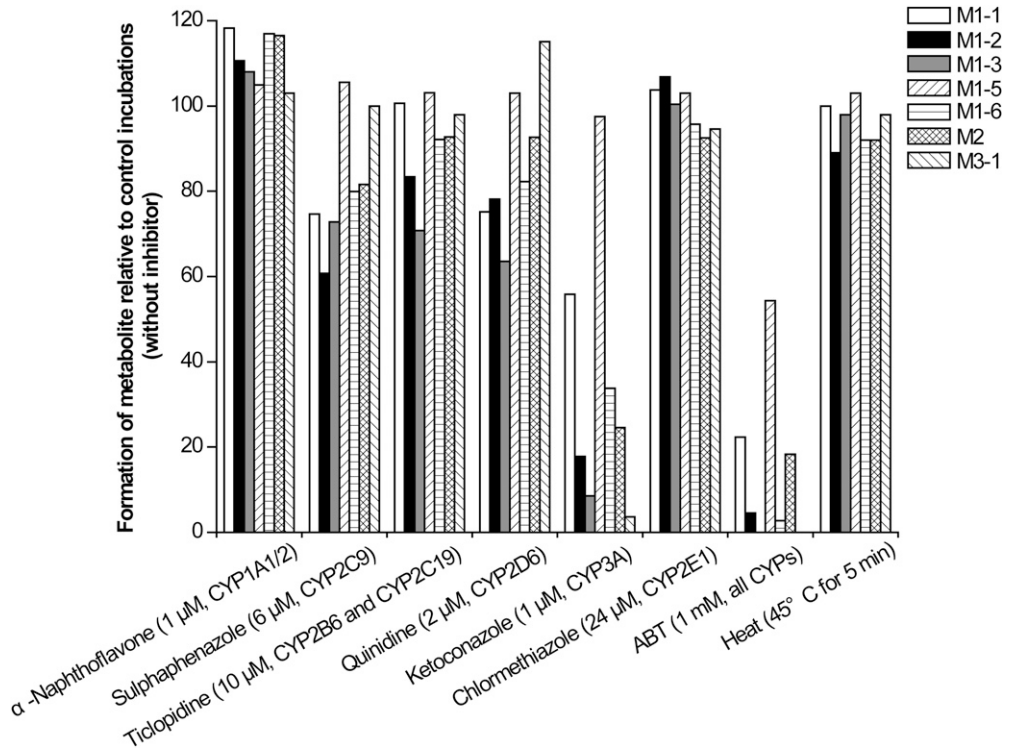

Fig. 7. Effect of P450 selective chemical inhibitors on the formation of major metabolites in HLMs. A 10-minute incubation and a final HLM concentration of 0.2 mg of protein/ml represented conditions that are linear and were used in this experiments. Each column represents the mean percentage activity relative to vehicle control from duplicate measurements.

of M1-1, M1-2, M1-6, M9-1, and M9-2 (based on molar concentrations) were approximately 40, 16, 21, 2, and 88% that of the parent drug, respectively.

After the last dose, the C_{max} values of apatinib, M1-1, M1-2, M1-6, M9-1, and M9-2 were achieved approximately 4.7 to 11.5 hours postdose, with mean values of 3935, 1470, 571, 786, 94.3, and 2843 nmol/l, respectively. During the first 24 hours after dosing, the systemic exposures of M1-1, M1-2, M1-6, M9-1, and M9-2 (based on molar concentrations) were approximately 56, 22, 32, 5, and 125% that of the parent drug, respectively. Therefore, M9-2 was the major circulating drug-related component at steady state, followed by parent drug, M1-1, M1-6, M1-2, and M9-1. The elimination half-life of apatinib, M1-1, M1-2, M1-6, M9-1, and M9-2 averaged 18.6, 24.7, 23.2, 21.2, 26.3, and 23.8 hours, respectively, indicating that systemic clearance for metabolites was slightly slower than that for the parent compound. After repeated administration, the $AUC_{0-24\ hour}$ accumulation ratios of apatinib and its metabolites were 1.77–3.69. The C_{max} accumulation ratios of apatinib and its metabolites

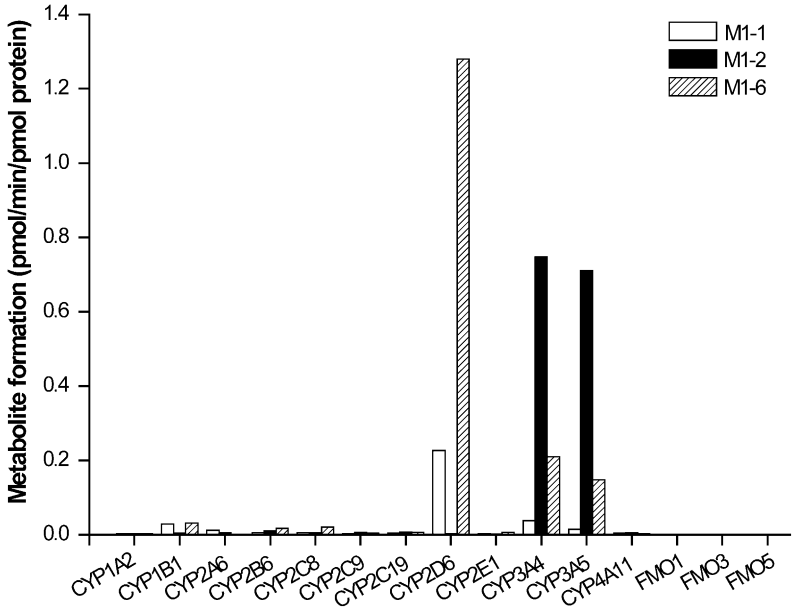

Fig. 8. Formation of M1-1, M1-2, and M1-6 from apatinib (2 μM) incubation in individual human recombinant P450 enzyme. Each bar represents the mean activity from duplicate measurements.

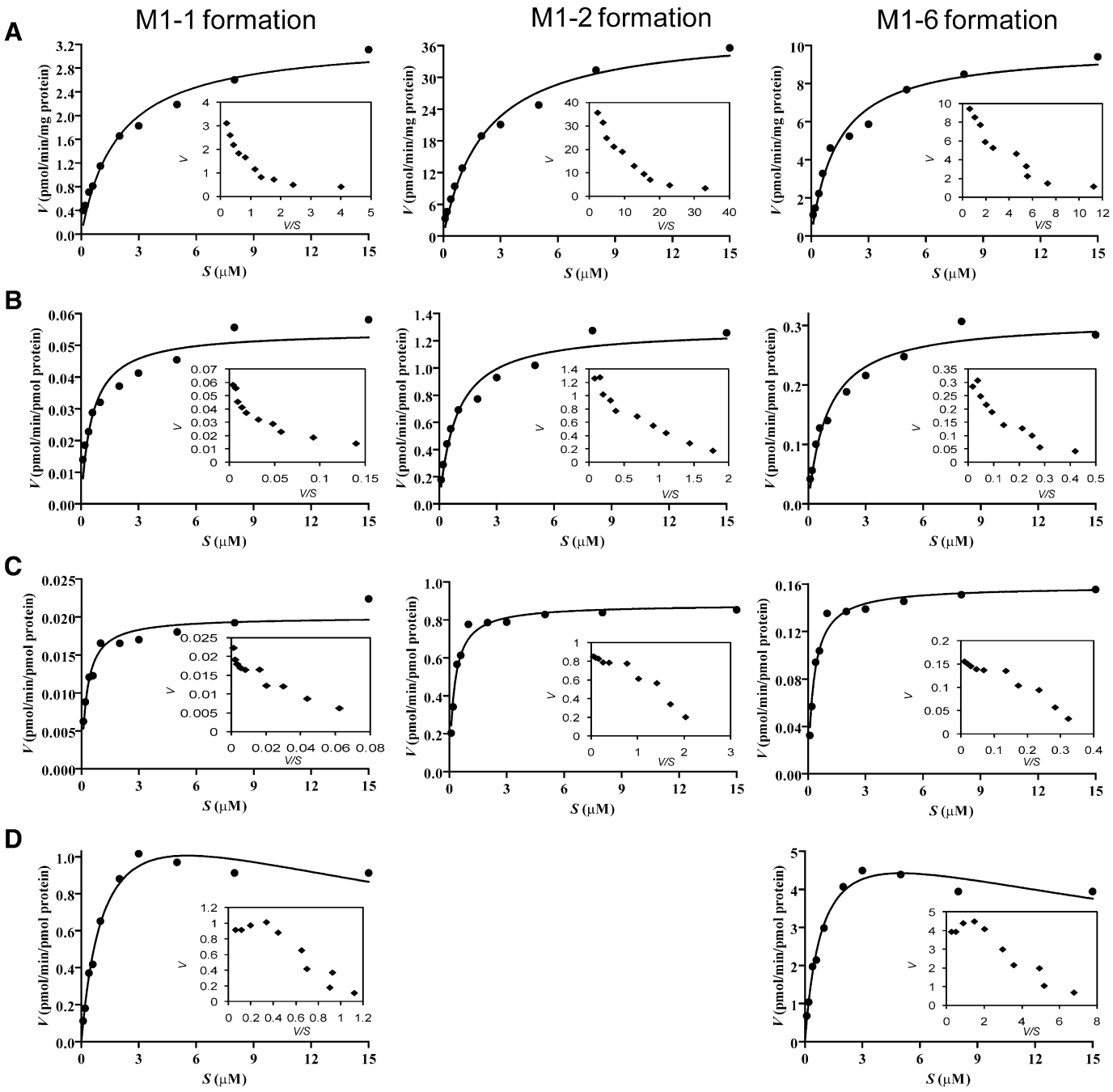

Fig. 9. Kinetic analysis for the formation of M1-1, M1-2, and M1-6 in HLMs (A), as well as human recombinant CYP3A4 (B), CYP3A5 (C), and CYP2D6 (D). Apatinib was incubated at concentrations in the range of 0.1–15 μM in triplicate.

were 1.16 to 3.01, respectively. Gender difference in the pharmacokinetics of apatinib in humans was not observed (unpublished data).

Excretion of Apatinib in Humans. The cumulative recovery of total drug-related compounds in urine, feces, and the sum of urine and feces after a single oral administration of 750 mg of apatinib mesylate to 12 healthy subjects is shown in Table 4. The total drug-related compounds were excreted predominantly in feces (69.8% ± 16.1% of dose), and only a minor proportion was excreted renally (7.02% ± 1.77% of dose). The average cumulative excretion was 76.8% ± 14.9%. As shown in Fig. 5, 59.0% of the administered dose was excreted as unchanged drug in feces. The metabolites M1-1, M1-2, M1-6, and total dioxygenated metabolites excreted in feces accounted for 2.76, 1.20, 0.02, and 6.80% of the administered dose, respectively. Unchanged apatinib was detected only in negligible quantities in urine. The metabolites M1-1, M1-2, M1-6, M4-7, M6-9, M6-10, M8-2, and M9-2 excreted in urine accounted for 0.567, 0.386, 0.982, 0.101, 0.472, 1.10, 1.87, and 1.53% of the dose, respectively. Gender difference in the excretion of apatinib was not observed.

Binding of Apatinib and Its Major Metabolites to Human Plasma Proteins. The percentage protein binding of apatinib, M1-1, M1-2, and M1-6 at concentrations in the range of therapeutic plasma levels are listed in Table 5.

TABLE 6

Kinetic parameters (mean ± S.D.) for the formation of M1-1, M1-2, and M1-6 in HLMs as well as in human recombinant CYP3A4, CYP3A5, and CYP2D6

Metabolite	Kinetic Parameters	HLM	CYP3A4	CYP3A5	CYP2D6
M1-1	K_m (μM)	1.93 ± 0.33	0.57 ± 0.13	0.28 ± 0.05	0.69 ± 0.15
	V_{max} [a]	3.28 ± 0.19	0.05 ± 0.003	0.02 ± 0.0007	1.07 ± 0.06
	CL_{int} [b]	1.70 ± 0.21	0.09 ± 0.02	0.07 ± 0.01	1.56 ± 0.29
	R^2	0.9726	0.9125	0.9318	0.9455
M1-2	K_m (μM)	2.18 ± 0.29	0.90 ± 0.15	0.26 ± 0.03	NA
	V_{max}	39.1 ± 1.79	1.29 ± 0.06	0.88 ± 0.02	NA
	CL_{int}	17.9 ± 1.74	1.44 ± 0.20	3.38 ± 0.35	NA
	R^2	0.9849	0.9644	0.9753	NA
M1-6	K_m (μM)	1.41 ± 0.22	1.02 ± 0.17	0.30 ± 0.03	0.53 ± 0.12
	V_{max}	9.82 ± 0.46	0.31 ± 0.01	0.16 ± 0.004	4.60 ± 0.24
	CL_{int}	7.01 ± 0.83	0.30 ± 0.04	0.52 ± 0.05	8.68 ± 1.61
	R^2	0.9765	0.9687	0.9792	0.9388

CL_{int}, intrinsic clearance; HLM, human liver microsome; K_m, Michaelis constant; NA, not applicable; R^2, calculated correlation coefficient.

[a]The unit for V_{max} was pmol/min/mg protein for HLM and pmol/min/pmol P450 for CYP3A4, CYP3A5, and CYP2D6.

[b]The unit for CL_{int} was μl/min/mg protein for HLM and μl/min/pmol P450 for CYP3A4, CYP3A5, and CYP2D6.

In Vitro Pharmacological Activity of Major Metabolites. In vitro pharmacological study results of major metabolites are listed in Table 5. M1-1 potently inhibited VEGFR-2, PDGFR-β, and c-kit with IC_{50} of 19, 47, and 125 nM, respectively. M1-2 moderately inhibited VEFGR-2, PDGFR-β, and c-kit with an IC_{50} of 179, 1352, and 2511 nM, respectively. M1-6 moderately inhibited VEFGR-2, PDGFR-β, and c-kit with IC_{50} of 265, 369, and 981 nM, respectively. M9-2 did not inhibit the kinase activity of either enzyme to any significant extent. The PAI values of M1-1 toward VEFGR-2, PDGFR-β, and c-kit were 5.42, 19.3, and 5.66% compared with parent drug, respectively. The PAI values of M1-2 and M1-6 toward VEFGR-2, PDGFR-β, and c-kit were all less than 1% compared with the parent drug.

Oxidative Metabolism of Apatinib in Microsomal and Cytochrome Enzyme Incubations. As shown in Fig. 6, after 1-hour microsomal or cytochrome enzyme incubations, approximately 50% of the parent compound was consumed in the HLM incubations, whereas only 13% was used in the HIM incubations. Apatinib was not metabolized by HRMs and HPMs. Therefore, the liver was suspected to be the major oxidative biotransformation site for apatinib. More than 95% of the parent compound was consumed in CYP2D6, CYP3A4, and CYP3A5 incubations. About 30 to 50% of the parent compound was consumed in CYP2C9 and CYP2E1 incubations, and about 5 to 15% of the parent compound was consumed in CYP1B1, CYP2C8, and CYP2C19 incubations. Less than 5% of the parent compound was consumed in CYP1A2, CYP2A6, CYP2B6, CYP4A11, FMO1, FMO3, and FMO5 incubations, indicating that these cytochrome and FMO enzymes contributed minimally to the metabolism of apatinib.

In an NADPH-dependent manner, apatinib was metabolized by HLMs into seven metabolites: M1-1, M1-2, M1-3, M1-5, M1-6, M2, and M3-1. M1-2 was the main in vitro metabolite based on the peak areas obtained. The absence of NADPH in the incubations implies the absence of any metabolites.

HLM Incubations in the Presence of Selective P450 Inhibitors. The inhibition results generated from selective chemical inhibitors on the formation of M1-1, M1-2, M1-3, M1-5, M1-6, M2, and M3-1 in HLM incubations are shown in Fig. 7. Compared with the control samples without inhibitors, incubation with α-naphthoflavone (CYP1A1/2 inhibitor) and chlormethiazole (CYP2E1 inhibitor) had no substantial effect on the formation of all the metabolites. Sulphaphenazole (CYP2C9 inhibitor) inhibited the formation of M1-1, M1-2, M1-3, M1-6,

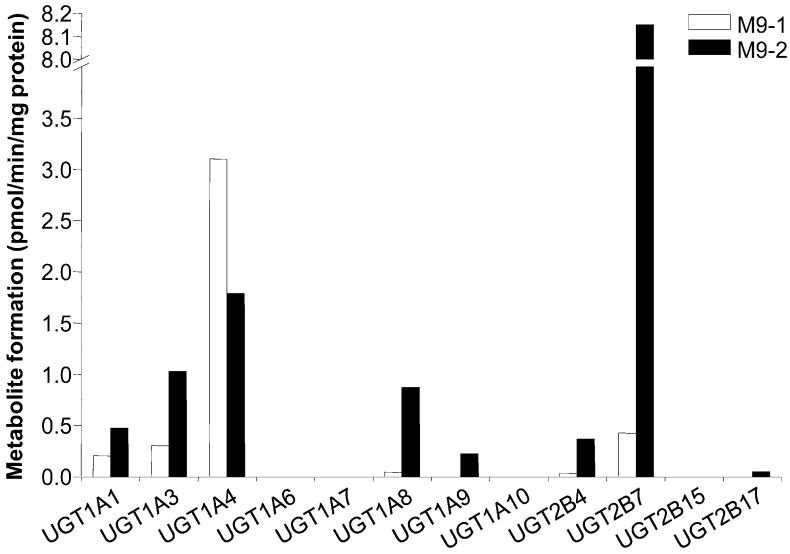

Fig. 10. *O*-Glucuronidation of M1-1 to form M9-2 (■) and M1-2 to form M9-1 (□) at substrate concentration of 20 μM by 12 human recombinant UGTs. Each column represents the mean of duplicate determinations.

and M2 by 18% to 39% and did not inhibit the formation of M1-5 and M3-1. Ticlopidine (inhibitor of CYP2B6 and CYP2C19) inhibited the formation of M1-2 and M1-3 by 17 and 29%, respectively, and did not inhibit the formation of other metabolites. Quinidine (CYP2D6 inhibitor) inhibited the formation of M1-1, M1-2, M1-3, and M1-6 by 18 to 36% and did not inhibit the formation of M1-5, M2, and M3-1. Ketoconazole (CYP3A4/5 inhibitor) inhibited the formation of M1-1, M1-2, M1-3, M1-6, M2, and M3 by 44, 82, 91, 66, 75, and 96%, respectively, but did not inhibit the formation of M1-5. ABT (inhibitor of all the cytochrome enzymes) inhibited the formation of M1-1, M1-2, M1-3, M1-5, M1-6, M2, and M3 by 78, 95, 100, 46, 97, 82, and 100%, respectively, suggesting the involvement of P450s in all metabolites yield. Heat treatment of HLM did not affect M1-6 (pridine-*N*-oxide) formation, thus excluding involvement of FMOs in M1-6 formation.

Formation of Major Oxidative Metabolites by Recombinant P450 Isoforms. As shown in Fig. 8, FMOs were not capable of apatinib metabolism. All tested cytochrome isoforms were capable of M1-1 and M1-2 formation. M1-1 was produced to the greatest extent by CYP2D6 (0.226 pmol/min/pmol protein) and to a lesser extent by CYP3A4 (0.037 pmol/min/pmol protein) and CYP3A5 (0.014 pmol/min/pmol protein). Other cytochromes also catalyzed the production of M1-1 but to much less extent. M1-2 was produced to the greatest extent by CYP3A4 (0.748 pmol/min/pmol protein) and CYP3A5 (0.710 pmol/min/pmol protein). M1-6 was predominantly formed by CYP2D6 (1.28 pmol/min/pmol protein) and to a lesser extent by CYP3A4 (0.210 pmol/min/pmol protein) and CYP3A5 (0.148 pmol/min/pmol protein).

In Vitro Enzyme Kinetic Study. The formation of M1-1, M1-2, and M1-6 by HLMs, CYP3A4, CYP3A5, and CYP2D6 exhibited Michaelis-Menten kinetics (Fig. 9). Table 6 presents the enzyme kinetic variables for the formation of M1-1, M1-2, and M1-6 in HLMs, CYP3A4, CYP3A5, and CYP2D6. V_{max} and K_m values for the formation of M1-1, M1-2, and M1-6 in CYP3A4 were all higher than that observed in CYP3A5, resulting in the comparable in vitro intrinsic clearance (V_{max}/K_m) in CYP3A4 and CYP3A5. The high V_{max} and CL_{int} values for the formation of M1-1 and M1-6 in CYP2D6 suggest that CYP2D6 has a high capability for the formation of M1-1 and M1-6. Enzyme kinetics of M1-2 formation in CYP2D6 was not determined because CYP2D6 catalyzed the formation of negligible M1-2.

Microsomal Conjugation of M1-1 and M1-2. M9-2 and M9-1 are *E*- and *Z*-isomers. M9-2 was the major circulating drug-related component at steady state, whereas M9-1 was present only in negligible quantities in human plasma. To investigate the selectivity, M1-1 and M1-2 were individually incubated with HLMs, HIMs, HPMs, and HRMs. *O*-glucuronidation of M1-1 to form M9-2 in the HLMs and HRMs was similar, whereas negligible amounts of M9-2 were formed in HIMs and HPMs (unpublished data). The highest M9-1 formation was observed in HLMs. The formation of M9-1 in HRMs was approximately 50% that in HLMs. Negligible amounts of M9-1 were formed in HIMs and HPMs (unpublished data). In HLMs, the formation of M9-2 was 8 times higher than that of M9-1. In HRMs, the formation of M9-2 was 16 times higher than that of M9-1.

UGT Enzymes Responsible for the Glucuronidation of M1-1 and M1-2. M1-1 and M1-2 were incubated with 12 individual UGT isoforms to identify the UGT enzymes responsible for the formation of M9-2 and M9-1 (Fig. 10). UGT1A1, UGT1A3, UGT1A4, UGT1A8, UGT1A9, UGT2B4, UGT2B7, and UGT2B17 all catalyzed the formation of M9-2, with UGT2B7 having the highest activity. UGT1A1, UGT1A3, UGT1A4, UGT1A8, UGT2B4, and UGT2B7 all catalyzed the formation of M9-1, with UGT1A4 having the highest activity, followed by UGT2B7. UGT2B7 is abundantly expressed in the liver, small intestine, colon, and kidney, whereas UGT1A4 is expressed only at relatively low levels in the liver (Ohno and Nakajin, 2009). Thus, both UGT1A4 and UGT2B7 may play important roles in the formation of M9-1.

The inhibitory effect of mefenamic acid (UGT2B7 inhibitor), racemic flubiprofen (UGT2B7 inhibitor), and hecogenin (UGT1A4 inhibitor) on the formation of M9-2 and M9-1 in HLMs was evaluated. As shown in Fig. 11, mefenamic acid inhibited M9-2 and M9-1 formation in HLMs with an IC_{50} of 2.64 μM (2.17–3.23 μM) and 8.35 μM (6.74–10.7 μM), respectively. Racemic flubiprofen inhibited M9-2 and M9-1 formation in HLMs with an IC_{50} of 13.6 μM (10.6–17.0 μM) and 44.4 μM (36.8–54.2 μM), respectively. Hecogenin showed little inhibitory effect on M9-2 formation. The IC_{50} of hecogenin was 45.7 μM (24.1–138 μM) for M9-1 formation. These results strongly suggest that UGT2B7 was the main enzyme

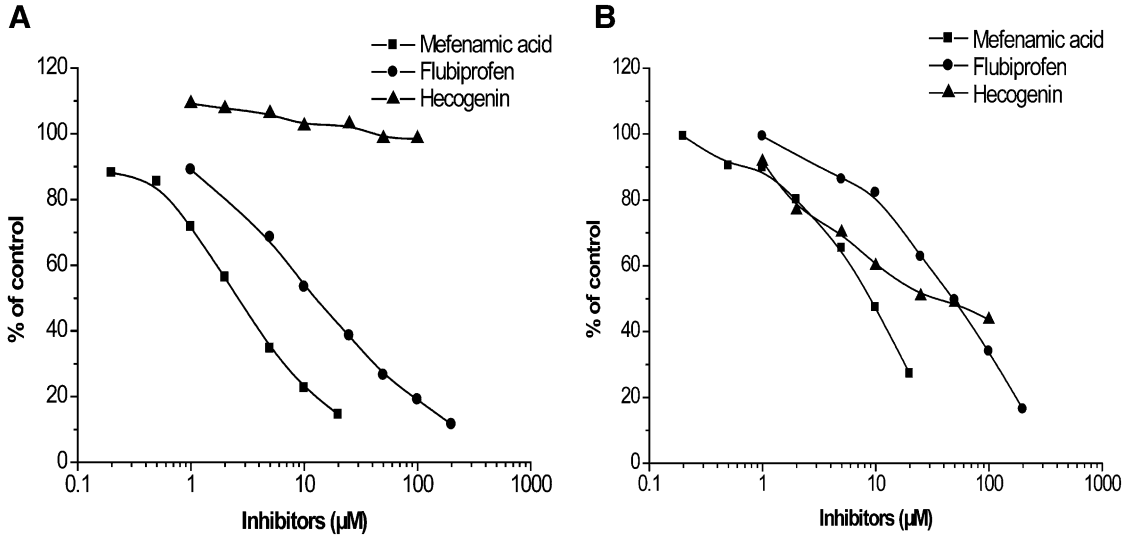

Fig. 11. Inhibitory effects of mefenamic acid, flurbiprofen, and hecogenin on the *O*-glucuronidation of M1-1 to form M9-2 (A) and M1-2 to form M9-1 (B) at a substrate concentration of 20 μM in HLMs. Data represent the mean of duplicate determinations.

responsible for M9-2 formation and that both UGT1A4 and UGT2B7 were responsible for M9-1 formation.

Discussion

The studies summarized in this article focus on the metabolism, pharmacokinetics, and excretion of apatinib after oral administration of 750 mg of apatinib mesylate to humans. Plasma samples for metabolism and pharmacokinetic analysis were collected from patients with advanced colorectal cancer. Urine and fecal samples for metabolism and excretion studies were collected from healthy subjects.

A total of 23, 35, and 14 metabolites were detected in human plasma, urine, and feces, respectively, by UPLC/Q-TOF MS. The proposed structures of the nine major metabolites M1-1, M1-2, M1-6, M4-7, M4-8, M6-9, M6-10, M8-2, and M9-2 were confirmed by comparison with reference standards after HPLC cochromatography, mass spectrometry, and NMR. The metabolic scheme of apatinib in humans is shown in Fig. 3. Systemically available apatinib was extensively metabolized in humans. The primary routes of apatinib biotransformation involved *E*- and *Z*-cyclopentyl-3-hydroxylation, *N*-dealkylation, pyridyl-25-*N*-oxidation, 16-hydroxylation, dioxygenation, and *O*-glucuronidation after cyclopentyl-3-hydroxylation. Apatinib shared some common metabolic pathways with its analog motesanib (Li et al., 2009), such as pyridyl-*N*-oxidation and *N*-dealkylation. However, the major metabolic reactions of apatinib occurred on the cyclopentyl group, including hydroxylation and further *O*-glucuronidation.

Total recovery of drug-related compounds accounted for 76.8% of the dose. Most of the recovered dose was eliminated via feces (69.8% of the dose). Only a minor proportion was excreted through urine (7.02% of the dose). About 59.0% of the total intake dose of apatinib was excreted unchanged within 0–96 hours via feces. The substantial fecal recovery of apatinib may be related to 1) nonabsorbed drug; 2) biliary excretion of apatinib; 3) unstable metabolites that convert back apatinib by intestinal bacterial enzymes after biliary transport into the intestine, such as the *N*-oxide (el-Mekkawy et al., 1993); or 4) direct intestinal excretion after absorption. Apatinib exhibited poor oral bioavailability after a single oral administration of apatinib mesylate to dogs (9.24% in male dogs, 15.4% in female dogs, unpublished data). Thus, the apatinib recovered in feces was suspected to represent mainly the nonabsorbed drug. In addition, the pyridyl-25-*N*-oxide metabolite (M1-6), which was found in plasma and urine, was detected only in negligible quantities in feces. These observations were in agreement with the reductive potential of human intestinal bacteria toward *N*-oxides. The excretion of M1-1, M1-2, M1-6, and total dioxygenated metabolites in feces accounted for 2.76, 1.20, 0.02, and 6.80% of the administered dose, respectively. Unchanged apatinib was detected only in negligible quantities in urine, indicating that the systemically available apatinib was extensively metabolized. The major metabolites M1-1, M1-2, M1-6, M4-7, M6-9, M6-10, M8-2, and M9-2 excreted in urine each accounted for less than 2% of the dose. Gender difference in the excretion of apatinib was not observed.

The major circulating metabolites may contribute to the overall efficacy and toxicity of the drug. Thus, determination of the pharmacokinetics of the major metabolites of a new drug is essential. The pharmacokinetics of unchanged apatinib in this study was comparable to data previously reported in cancer patients (Li et al., 2010). C_{max} of apatinib was achieved 2.9 to 4.7 hour postdose. Significant interpatient variability with apatinib indicated that dose modification may be needed to meet individual needs. The major circulating metabolite was the pharmacologically inactive metabolite M9-2, the steady-state exposure of which was 125% that of the parent drug at steady state. The systemic exposures of M1-1, M1-2, and M1-6 were 56, 22, and 32% that of the parent drug, respectively. Calculated as PAI values, the contribution of M1-1 to the pharmacology of the drug was 5.42 to 19.3% that of the parent drug, and the contribution of M1-2 and M1-6 to the pharmacology of the drug was less than 1% that of the parent drug. Therefore, among the prominent systemically available drug-related components, the parent drug was considered to have major contributions to the overall pharmacological activity in humans; active mono-oxygenated metabolites M1-1, M1-2, and M1-6 were considered to have only minor contributions. The systemic clearance for all the metabolites quantified was slightly slower than that for the parent drug. The accumulation degrees of apatinib and its metabolites were observed to be moderate, with mean $AUC_{0-24\ hour}$ accumulation ratios ranging from 1.77 to 3.69.

The oxidative metabolites of apatinib were formed mainly in the liver in an NADPH-dependent manner. In vitro metabolism studies with recombinant human isozymes and inhibition studies with selective chemical inhibitors of human P450 enzymes demonstrated that the oxidative metabolism of apatinib was mediated by CYP3A4/5 and, to a lesser extent, by CYP2D6, CYP2C9, and CYP2E1. All tested cytochrome isoforms were capable of M1-1 and M1-2 formation. M1-1 was produced to the greatest extent by CYP2D6 and to a lesser extent by CYP3A4 and CYP3A5. M1-2 was produced to the greatest extent by CYP3A4 and CYP3A5. M1-6 was predominantly formed by CYP2D6 and to a lesser extent by CYP3A4 and CYP3A5. *N*-dealkylation of apatinib was mediated predominantly by CYP3A4/5. Hydroxylation and dealkylation are most common metabolic pathways observed in CYP2D6 substrates, whereas *N*-oxidation is far less common in CYP2D6 substrate. However, there are a few prior examples of CYP2D6-mediated formation of *N*-oxide. Procainamide (Lessard et al., 1999), sparteine (Zhou et al., 2009), citalopram (Olesen et al., 1999), AZD0328 {(2′*R*)-spiro[1-azabicyclo[2.2.2]octane-3,2′(3′H)-furo[2,3-b]pyridine]} (Zhou et al., 2011), and another AZD0328 structure similar α7 NNR agonist {*N*-(3*R*)-1-azabicyclo[2.2.2]oct-3-ylfuro[2,3-*c*]pyridine-5-carboxamide} (Shaffer et al., 2007) probably are the only limited number of compounds reported previously to have *N*-oxidation catalyzed by CYP2D6.

The kinetic analysis indicated higher V_{max} but lower binding affinity for the formation of M1-1, M1-2, and M1-6 in CYP3A4 than that observed in CYP3A5, indicating the comparable in vitro intrinsic clearance (V_{max}/K_m) in CYP3A4 and CYP3A5. Although CYP2D6 has a higher capability for the formation of M1-1 and M1-6 than CYP3A4 and CYP3A5, results of the in vitro inhibition studies with selective chemical inhibitors indicated that CYP2D6 are not expected to play a significant role in the hepatic clearance of apatinib in humans.

The concomitance of known CYP3A4/5 inducers, inhibitors, or substrate may influence drug levels of apatinib. Further in vivo studies will be conducted to evaluate the clinical drug-drug interaction. Hypertension is observed as an adverse effect of all the oral VEGF tyrosine kinase inhibitors (Izzedine et al., 2007), which have occurred because the inhibition of VEGFR in arterial endothelial cells decreases the release of nitric oxide (Tang et al., 2004). In phase 1 clinical studies of apatinib, 68% of the patients who took the drug experienced hypertension. Many antihypertensive drugs, such as amlodipine, diltiazem, felodipine, nicardipine, nifedipine, and verapamil, were the substrates or inhibitors of CYP3A. Thus, the concomitant use of these antihypertensive medications with apatinib in patients may induce drug-drug interactions. The potential for drug interactions with M1-1 and M1-6 (metabolite present at greater than 25% of parent drug AUC) should be considered in the following studies according to Food

and Drug Administration guidance (http://www.fda.gov/downloads/Drugs/GuidanceComplianceRegulatoryInformation/Guidances/UCM292362.pdf).

M9-2 (*O*-glucuronide of M1-1) and M9-1 (*O*-glucuronide of M1-2) were *E*- and *Z*-isomers. Measured as $AUC_{0-24\ hour}$ ratios at steady state, the plasma exposure of M1-1 was 1.6-fold higher than that of M1-2, whereas the plasma exposure of M9-2 was 25.6-fold higher than that of M9-1. These observations suggested that the formation of M9-2 is preferred over M9-1. To test this, M1-1 and M1-2 were individually incubated with HLMs, HIMs, HPMs, and HRMs. Both liver and kidney were found to be important biotransformation sites for the formation of M9-2 and M9-1. In HLMs, the formation of M9-2 was 8 times higher than that of M9-1. In HRMs, the formation of M9-2 was 16 times higher than that of M9-1. These observations were in agreement with the preference in vivo. Incubations with recombinant human UGTs and inhibition studies with selective chemical inhibitors suggested that UGT2B7 was the major UGT isozyme catalyzing the formation of M9-2; UGT1A4 and UGT2B7 were both important UGT isozymes catalyzing the formation of M9-1.

M1-1 (*E*-3-hydroxy-apatinib) and M1-2 (*Z*-3-hydroxy-apatinib) were *E*- and *Z*-isomers. Measured as $AUC_{0-24\ hour}$ ratios at steady state, M1-1 was 1.6 times greater than M1-2, and the sum of M1-1 and its *O*-glucuronide conjugate (M9-2) was 5.87 times higher than the sum of M1-2 and its *O*-glucuronide conjugate (M9-1). M1-1 in urine and feces was also higher than M1-2. Therefore, a preference was identified in humans for the formation of M1-1 to its *Z*-isomer M1-2. However, the in vitro microsomal incubation studies and the chemical oxidative reactions both showed a preference for the formation of the *Z*-isomer M1-2. Further investigation is needed to reveal the exact causes.

Acknowledgments

The authors thank Liguang Lou for kind assistance on the assay of the in vitro pharmacological activity of the major metabolites of apatinib. The clinical studies were conducted at Teda International Cardiovascular Hospital (Tianjin, China) and Fudan University Shanghai Cancer Center (Shanghai, China).

Authorship Contributions

Participated in research design: Ding, Zhong, Chen, Jiang, Zhang.
Conducted experiments: Ding, Li, Gao, Dai, Xie.
Contributed new reagents or analytic tools: Ding, Zhong, Chen.
Performed data analysis: Ding, Zhong, Chen, Gao, Li.
*Contributed to the writing of the manu*script: Ding, Zhong.

References

Carmeliet P and Jain RK (2000) Angiogenesis in cancer and other diseases. *Nature* **407**:249–257.
Chelucci G, Baldino S, Pinna GA, Benaglia M, Buffa L, and Guizzetti S (2008) Chiral pyridine *N*-oxides derived from monoterpenes as organocatalysts for stereoselective reactions with allyltrichlorosilane and tetrachlorosilane. *Tetrahedron* **64**:7574–7582.
Degrauwe N, Sosa JA, Roman S, and Deshpande HA (2012) Vandetanib for the treatment of metastatic medullary thyroid cancer. *Clin Med Insights Oncol* **6**:243–252.
Ding J, Chen X, Dai X, and Zhong D (2012) Simultaneous determination of apatinib and its four major metabolites in human plasma using liquid chromatography-tandem mass spectrometry and its application to a pharmacokinetic study. *J Chromatogr B Analyt Technol Biomed Life Sci* **895-896**:108–115.
el-Mekkawy S, Meselhy MR, Kawata Y, Kadota S, Hattori M, and Namba T (1993) Metabolism of strychnine *N*-oxide and brucine *N*-oxide by human intestinal bacteria. *Planta Med* **59**: 347–350.
Gennigens C and Jerusalem G (2012) [Pazopanib (Votrient) in the management of renal cell cancer and soft tissue sarcomas]. *Rev Med Liege* **67**:437–442.
Glade-Bender J, Kandel JJ, and Yamashiro DJ (2003) VEGF blocking therapy in the treatment of cancer. *Expert Opin Biol Ther* **3**:263–276.
Heinrich MC, Blanke CD, Druker BJ, and Corless CL (2002) Inhibition of KIT tyrosine kinase activity: a novel molecular approach to the treatment of KIT-positive malignancies. *J Clin Oncol* **20**:1692–1703.
Hunt JT, Mitt T, Borzilleri R, Gullo-Brown J, Fargnoli J, Fink B, Han WC, Mortillo S, Vite G, and Wautlet B,, et al. (2004) Discovery of the pyrrolo[2,1-f][1,2,4]triazine nucleus as a new kinase inhibitor template. *J Med Chem* **47**:4054–4059.
Irby RB and Yeatman TJ (2000) Role of Src expression and activation in human cancer. *Oncogene* **19**:5636–5642.
Ivy SP, Wick JY, and Kaufman BM (2009) An overview of small-molecule inhibitors of VEGFR signaling. *Nat Rev Clin Oncol* **6**:569–579.
Izzedine H, Rixe O, Billemont B, Baumelou A, and Deray G (2007) Angiogenesis inhibitor therapies: focus on kidney toxicity and hypertension. *Am J Kidney Dis* **50**:203–218.
Kulanthaivel P, Barbuch RJ, Davidson RS, Yi P, Rener GA, Mattiuz EL, Hadden CE, Goodwin LA, and Ehlhardt WJ (2004) Selective reduction of N-oxides to amines: application to drug metabolism. *Drug Metab Dispos* **32**:966–972.
Leclercq L, Cuyckens F, Mannens GS, de Vries R, Timmerman P, and Evans DC (2009) Which human metabolites have we MIST? Retrospective analysis, practical aspects, and perspectives for metabolite identification and quantification in pharmaceutical development. *Chem Res Toxicol* **22**:280–293.
Lessard E, Hamelin BA, Labbé L, O'Hara G, Bélanger PM, and Turgeon J (1999) Involvement of CYP2D6 activity in the N-oxidation of procainamide in man. *Pharmacogenetics* **9**:683–696.
Li C, Kuchimanchi M, Hickman D, Poppe L, Hayashi M, Zhou Y, Subramanian R, Kumar G, and Surapaneni S (2009) In vitro metabolism of the novel, highly selective oral angiogenesis inhibitor motesanib diphosphate in preclinical species and in humans. *Drug Metab Dispos* **37**:1378–1394.
Li J, Zhao X, Chen L, Guo H, Lv F, Jia K, Yv K, Wang F, Li C, and Qian J, et al. (2010) Safety and pharmacokinetics of novel selective vascular endothelial growth factor receptor-2 inhibitor YN968D1 in patients with advanced malignancies. *BMC Cancer* **10**:529–536.
Mano Y, Usui T, and Kamimura H (2007a) Predominant contribution of UDP-glucuronosyltransferase 2B7 in the glucuronidation of racemic flurbiprofen in the human liver. *Drug Metab Dispos* **35**: 1182–1187.
Mano Y, Usui T, and Kamimura H (2007b) The UDP-glucuronosyltransferase 2B7 isozyme is responsible for gemfibrozil glucuronidation in the human liver. *Drug Metab Dispos* **35**: 2040–2044.
Mi YJ, Liang YJ, Huang HB, Zhao HY, Wu CP, Wang F, Tao LY, Zhang CZ, Dai CL, and Tiwari AK, et al. (2010) Apatinib (YN968D1) reverses multidrug resistance by inhibiting the efflux function of multiple ATP-binding cassette transporters. *Cancer Res* **70**:7981–7991.
Ohno S and Nakajin S (2009) Determination of mRNA expression of human UDP-glucuronosyltransferases and application for localization in various human tissues by real-time reverse transcriptase-polymerase chain reaction. *Drug Metab Dispos* **37**:32–40.
Olesen OV and Linnet K (1999) Studies on the stereoselective metabolism of citalopram by human liver microsomes and cDNA-expressed cytochrome P450 enzymes. *Pharmacology* **59**: 298–309.
Shaffer CL, Gunduz M, Scialis RJ, and Fang AF (2007) Metabolism and disposition of a selective $\alpha(_7)$ nicotinic acetylcholine receptor agonist in humans. *Drug Metab Dispos* **35**:1188–1195.
Smith DA and Obach RS (2005) Seeing through the mist: abundance versus percentage: commentary on metabolites in safety testing. *Drug Metab Dispos* **33**:1409–1417.
Song S, Ewald AJ, Stallcup W, Werb Z, and Bergers G (2005) PDGFRbeta+ perivascular progenitor cells in tumours regulate pericyte differentiation and vascular survival. *Nat Cell Biol* **7**: 870–879.
Tang JR, Markham NE, Lin YJ, McMurtry IF, Maxey A, Kinsella JP, and Abman SH (2004) Inhaled nitric oxide attenuates pulmonary hypertension and improves lung growth in infant rats after neonatal treatment with a VEGF receptor inhibitor. *Am J Physiol Lung Cell Mol Physiol* **287**:L344–L351.
Tian S, Quan H, Xie C, Guo H, Lü F, Xu Y, Li J, and Lou L (2011) YN968D1 is a novel and selective inhibitor of vascular endothelial growth factor receptor-2 tyrosine kinase with potent activity in vitro and in vivo. *Cancer Sci* **102**:1374–1380.
Tong XZ, Wang F, Liang S, Zhang X, He JH, Chen XG, Liang YJ, Mi YJ, To KK, and Fu LW (2012) Apatinib (YN968D1) enhances the efficacy of conventional chemotherapeutical drugs in side population cells and ABCB1-overexpressing leukemia cells. *Biochem Pharmacol* **83**: 586–597.
Tugnait M, Hawes EM, McKay G, Rettie AE, Haining RL, and Midha KK (1997) N-oxygenation of clozapine by flavin-containing monooxygenase. *Drug Metab Dispos* **25**:524–527.
Uchaipichat V, Mackenzie PI, Elliot DJ, and Miners JO (2006) Selectivity of substrate (trifluoperazine) and inhibitor (amitriptyline, androsterone, canrenoic acid, hecogenin, phenylbutazone, quinidine, quinine, and sulfinpyrazone) "probes" for human udp-glucuronosyltransferases. *Drug Metab Dispos* **34**:449–456.
Verbeke N, Pellegrin P, Vienne A, and Lesne M (1979) The binding of gitoxin to human plasma proteins. *Eur J Clin Pharmacol* **16**:341–344.
Zhang H, Zhu M, Ray KL, Ma L, and Zhang D (2008) Mass defect profiles of biological matrices and the general applicability of mass defect filtering for metabolite detection. *Rapid Commun Mass Spectrom* **22**:2082–2088.
Zhou D, Zhang M, Ye X, Gu C, Piser TM, Lanoue BA, Schock SA, Cheng YF, and Grimm SW (2011) In vitro metabolism of α7 neuronal nicotinic receptor agonist AZD0328 and enzyme identification for its *N*-oxide metabolite. *Xenobiotica* **41**:232–242.
Zhou SF, Liu JP, and Lai XS (2009) Substrate specificity, inhibitors and regulation of human cytochrome P450 2D6 and implications in drug development. *Curr Med Chem* **16**:2661–2805.

Address correspondence to: Dr. Dafang Zhong, Shanghai Institute of Materia Medica, Chinese Academy of Sciences, 501 Haike Road, Shanghai 201203, P.R. China. E-mail: dfzhong@mail.shcnc.ac.cn